CHARACTERIZATION OF *VIBRIO PARAHAEMOLYTICUS*-INDUCED INTESTINAL INFLAMMATION IN THE MOUSE

APPROVED BY SUPERVISORY COMMITTEE

_____

_____

_____

_____

CHARACTERIZATION OF *VIBRIO PARAHAEMOLYTICUS*-INDUCED INTESTINAL INFLAMMATION IN THE MOUSE

by

OLIVIA LEE

DISSERTATION

Presented to the Faculty of the Graduate School of Biomedical Sciences

The University of Texas Southwestern Medical Center at Dallas

In Partial Fulfillment of the Requirements

For the Degree of

DOCTOR OF PHILOSOPHY

The University of Texas Southwestern Medical Center at Dallas

Dallas, Texas

July 2009

CHARACTERIZATION OF *VIBRIO PARAHAEMOLYTICUS*-INDUCED INTESTINAL INFLAMMATION IN THE MOUSE

OLIVIA LEE, Ph.D.

The University of Texas Southwestern Medical Center at Dallas, 2009

KIM ORTH, Ph.D.

The Gram-negative marine bacterium *Vibrio parahaemolyticus* is a leading cause of gastroenteritis from the consumption of contaminated seafood. Some recent outbreaks are attributed to a rise in ocean temperatures, a trend that is likely to continue as a result of global warming and emphasizes the need to study the virulence mechanisms of the pathogen. *V. parahaemolyticus* utilizes a type III secretion system to inject effectors that disrupt signal transduction in eukaryotic hosts during infection. Herein, we describe an *in vivo* model of infection by *V. parahaemolyticus* using germfree mice. *V. parahaemolyticus* is

recovered from the cecum and colon of mice infected by oral gavage. Mice infected with a pathogenic, wild type strain of *V. parahaemolyticus* exhibit intestinal inflammation characterized by epithelial damage, submucosal edema, crypt abscess and hyperplasia, and infiltration of the lamina propria by neutrophils. Using mutant strains of *V. parahaemolyticus*, we have determined that thermostable direct hemolysin, the most well characterized virulence factor produced by *V. parahaemolyticus*, and T3SS2, one of the two type III secretion systems present in this bacterium, both contribute to enteropathogenesis. Analysis of the expression of inflammatory cytokines IL-1β and IFN-γ and chemokines KC, MIP-2α, and CXCL-9 reveals that the duration of the inflammatory response is extended in the presence of TDH. In addition to delineating the roles of the virulence factors TDH, type III secretion system 1, and type III secretion system 2, in the infection process, we have developed an experimental system that will enable further characterization of type III effectors of *V. parahaemolyticus.*

TABLE OF CONTENTS

LIST OF FIGURES

CHAPTER ONE
Introduction

Vibrio parahaemolyticus

Vibrio parahaemolyticus is a Gram-negative, rod-shaped, halophilic bacterium commonly found in marine and estuarine environments [10]. *V. parahaemolyticus* is free living in these environments but can also be found in close association with fish, shellfish, and planktonic copepods [18, 31, 32].

Worldwide, *V. parahaemolyticus* is a leading cause of gastroenteritis due to the consumption of contaminated seafood [82]. In 1950, the bacterium was first identified as the etiologic agent of an outbreak of food poisoning in Osaka, Japan that encompassed 272 cases of acute gastroenteritis, 20 of which were fatal [18]. The first documented U.S. outbreak of *V. parahaemolyticus* infection occurred in 1971 and was attributed to the consumption of contaminated crabmeat in Maryland [40].

Following its discovery as an etiologic agent of gastroenteritis, outbreaks of *V. parahaemolyticus* infection were sporadic and attributed to a number of different strains [40]. In 1996, however, a jump in the incidence of reported cases in Calcutta, India led to the discovery of the O3:K6 serotype, which has since been attributed to a number of outbreaks worldwide [43]. The emergence of O3:K6 and other pandemic strains has also been compounded by a global rise in ocean temperature, as demonstrated by the incidence of an infectious outbreak in

Alaska, where water temperatures were previously thought to be too low to support the viability of *V. parahaemolyticus* [38].

Human Diseases Caused by *V. parahaemolyticus*

Infection by *V. parahaemolyticus* can result in wound infections or septicemia, particularly in individuals with compromised liver function. [82]. However, the most common illness associated with infection by *V. parahaemolyticus* is acute, self-limiting gastroenteritis. Symptoms persist for approximately 3 days and may include diarrhea, abdominal cramps, nausea, vomiting, fever, and headache [82]. Histopathological examination of duodenal tissue isolated from patients infected with *V. parahaemolyticus* revealed acute inflammation characterized by compromised epithelial integrity, disruption of the villous architecture, and infiltration of crypts and villi by polymorphonuclear leukocytes (PMNs) [48].

TDH and TRH

Most clinical isolates of *V. parahaemolyticus* demonstrate the ability to cause β-hemolysis on Wagatsuma blood agar [39]. This activity, termed the Kanagawa phenomenon (KP), is a hallmark of pathogenic strains and is attributed to thermostable direct hemolysin (TDH), a pore-forming toxin [28] that remains the most well characterized virulence factor produced by *V. parahaemolyticus* to

date. TDH is a protein dimer composed of two subunits, each with a molecular mass of 21 kDa [69]. Multiple copies of *tdh,* the gene that encodes TDH protein, may be present within the genome of *V. parahaemolyticus* and influence the hemolytic phenotype in a strain-specific manner. For example, the majority of KP-positive strains contain two copies of *tdh*, designated *tdh1* and *tdh2*, whereas weakly KP-positive and some KP-negative strains possess only a single copy [35].

The mechanistic contribution of TDH to the virulence of *V. parahaemolyticus* is still not entirely clear. Fluid accumulation in the ileal loop of rabbits is often measured as a gauge of enterotoxicity, and experiments utilizing whole cultures of *V. parahaemolyticus* revealed a correlation between KP-positive strains and fluid accumulation [57, 72]. *In vitro*, TDH has been found to be cytotoxic to a number of cultured cell types, including human amniotic membrane cells [58], human embryonic cells {Tang, 1995 #44}, and human intestinal epithelial cells [50]. Additional studies in cultured rat crypt small intestinal (IEC-6) monolayers suggest that the pore-forming capabilities of TDH effect a transient increase in levels of intracellular calcium [17]. The alterations in cellular ion flux are thought to contribute to decreased reabsorption of water in the large intestine, resulting in the diarrhea that is associated with infection by *V. parahaemolyticus*.

While TDH and a KP-positive phenotype are strongly associated with pathogenicity in *V. parahaemolyticus*, an outbreak of gastroenteritis in the

Republic of Maldives resulted in the isolation of a pathogenic, KP-negative strain of *V. parahaemolyticus* [26]. Analysis of this strain resulted in the discovery of a second hemolysin, TDH-related hemolysin (TRH), that bears 67% homology to TDH [27]. From analysis by the rabbit ileal loop test, TRH was found to induce fluid secretion [27]. The link between the hemolysins and gastroenteritis-associated diarrhea is reinforced by the finding that both TDH and TRH are able to stimulate chloride secretion in cultured colonic epithelial cells [67, 68].

In spite of the seemingly clear correlation between hemolysins and the pathogenicity of *V. parahaemolyticus*, some rabbit ileal loop studies suggested the requirement of an additional virulence factor or toxin for pathogenicity [73]. The discovery, coincident with sequencing of the genome of the clinical strain RIMD2210633, of two type III secretion systems (T3SS) in *V. parahaemolyticus* [36], provided several avenues for the study of additional virulence mechanisms.

The Type III Secretion Sytem

Studies on the virulence factor YopE from *Yersinia pestis*, the causative agent of bubonic plague, demonstrated that contact between the pathogen and the surface of a eukaryotic host cell initiated a series of events culminating in the polarized translocation of YopE into the host cytoplasm [56]. The mechanism through which this translocation occurs was later termed type three secretion and is mediated by the T3SS, a conserved needle-like apparatus comprising approximately 20 proteins (reviewed in [19]). The needle complex central to the

T3SS, first identified in *Salmonella typhimurium* [33], consists of a ringed base that attaches to the bacterial envelope, a needle-like projection that extends beyond the surface of the cell, and a central inner rod structure that connects the needle and base [19]. The complex is traversed by a channel with a diameter of approximately 28 Å, through which bacterial proteins are translocated into the host cell[19].

The bacterial proteins, termed effectors, which are injected into eukaryotic cells via the T3SS may be considered the bacterial equivalent of viral oncogenes based on a number of characteristics. Most type three effectors evade detection by the host cell through the mimicking or capture of an endogenous eukaryotic activity and, in doing so, disrupt eukaryotic signaling pathways that might otherwise be activated in response to infection. YopE, for example, possesses GTPase-activating protein (GAP) activity against members of the Rho family of GTPases [75]. Consequent inactivation of these Rho GTPases results in cell rounding, disruption of actin filaments, and inhibition of phagocytosis [5, 54, 55]. These and other T3SS effector-mediated disruptions thus facilitate the survival and replication of the bacterium within the host.

In 2003, Makino *et al* published the genome sequence of RIMD2210633, a strain of *V. parahaemolyticus* isolated from the stool of a patient diagnosed with travelers' diarrhea [36]. RIMD2210633 was characterized as a KP-positive, TDH-positive, TRH-negative strain of *V. parahaemolyticus* that possesses two

circular chromosomes [36]. Chromosome 1 is approximately 3.3 x 10^6 bp in length, while chromosome 2 is approximately 1.9 x 10^6 bp in length [36]. Chromosome 1 was found to contain a set of genes encoding ~30 T3SS-related genes, beginning 1.7 x 10^6 bp from the origin of replication [36]. This T3SS, designated T3SS1, has also been identified in all clinically and environmentally isolated strains tested to date [36]. Chromosome 2 of RIMD2210633 was also found to contain a T3SS, designated T3SS2, located on a ~80 kb pathogenicity island (PAI) on which the *tdh* genes were also identified [36]. However, unlike T3SS1, the presence of T3SS2 and the PAI correlate only with pathogenic strains of *V. parahaemolyticus* [36]. Further genomic analysis revealed the G+C content of the PAI to be 39.8%, compared to 45.4% in the rest of the genome, suggesting that the PAI was acquired by lateral transfer more recently than the remainder of the genome [36]. Functional analysis of T3SS1 and T3SS2 from *V. parahaemolyticus* revealed distinct roles for each T3SS. Studies in cell culture suggest that T3SS1 is responsible for the cytotoxic effects of *V. parahaemolyticus*. Infection of HeLa cells with a strain of *V.* parahaemolyticus in which effectors are secreted only from T3SS1 results in cell death mediated by autophagy, cell rounding, and then cell lysis [9, 34]. These three events, which are separate but occur in parallel, are thought to be attributed to the cumulative functions of discrete T3SS1 effectors.

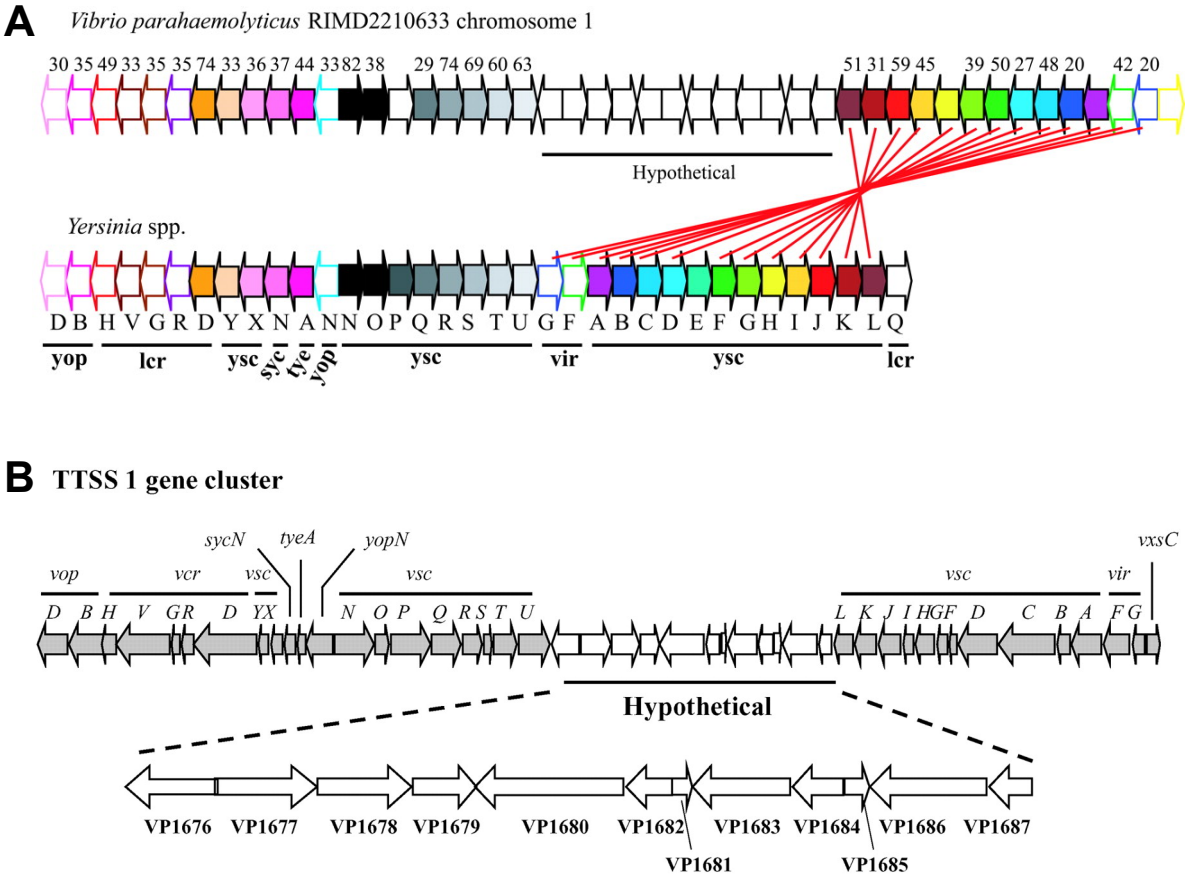

Figure 1. Organization of *V. parahaemolyticus* T3SS1

(A) Schematic representations of T3SS1 from *V. parahaemolyticus* (top) and the T3SS from *Yersinia* spp. Corresponding colors indicate homologous genes and the percent homology is denoted by numbers above *V. parahaemolyticus* T3SS1. Intersecting red lines indicate the reverse orientation of these genes in T3SS1 relative to their counterparts in *Yersinia* spp. A region of hypothetical genes in T3SS1 is underlined (A) and expanded in (B). Predicted effectors are encoded by the genes *vp1680* (VopQ), *vp1683* (VopR), and *vp1686* (VopS). Each effector is adjacent to its corresponding chaperone: *vp1682*, *vp1684*, and *vp1687*, respectively. Modified from [44, 46].

Type III Effectors of *V. parahaemolyticus*

Several of the genes on T3SS1 bear homology to, and are organized in a similar fashion as, T3SS genes from bacteria of the genus *Yersinia* (Fig. 1A). However, thirteen genes, spanning *vscL1* to *virG1*, are oriented in the direction opposite their counterparts from *Yersinia* [46]. T3SS1 also contains a region of 12 hypothetical genes located between *vscU1* and *vscL1*, the respective *V. parahaemolyticus* homologs of *Yersinia yscU* and *yscL* [46]. Based on their association with putative chaperone proteins, the products of three of these hypothetical genes—VP1680, VP1683, and VP1686—were identified as T3SS effectors [15] and have subsequently been renamed VopQ (VP1680), VopR (VP1683), and VopS (VP1686). VopQ has been implicated in the induction of autophagy in infected cells ([9] and unpublished data), while the biochemical function of VopR remains to be determined. It was recently determined that VopS interacts with and modifies members of the Rho family of guanosine triphosphatases (GTPases) by the covalent addition of adenosine 5'-monophosphate (AMP) to a conserved threonine residue [81]. This modification, termed AMPylation, inhibits downstream signaling by the Rho GTPases and thus interferes with actin assembly in the infected cell [81].

Based on their genetic similarity to known effectors from other bacterial species, more is known about the effectors located on T3SS2 than those on

T3SS1. VopC (VPA1321) and VopT (VPA1327) bear homology to *Escherichi coli* cytotoxic necrotizing factor (CNF-1) and *Pseudomonas aeruginosa* exoenzyme T (ExoT), respectively [36] [70]. While the mechanism of VopC has not been determined explicitly, it is thought to be similar to that of CNF-1, which deamidates the glutamine residue at position 63 of the small GTPase Rho in order to inhibit the intrinsic GTPase activity and constitutively activate Rho [60]. In *P. aeruginosa,* ExoT and the related protein ExoS are bifunctional enzymes that possess RhoGAP activity at the N terminus and ADP ribosylation activity at the C terminus (reviewed in [16]). While VopT does not align with the GAP domain of ExoT or ExoS, VopT does bear approximately 45% sequence similarity to the ADP ribosyltransferase domain of these proteins and functions as an ADP-ribosyltransferase [70]. VopA (VPA1346) is homologous to the *Yersinia spp.* effector YopJ, which has been shown to acetylate two conserved amino acid residues located in the activation loop of mitogen activated protein kinase kinases (MKKs) [41]. Acetylation prevents the phosphorylation and subsequent activion of these MKKs, thus disrupting signaling cascades involved in mediating the inflammatory response [41]. VopA behaves in a highly similar fashion but acetylates a third amino acid residue, Lys-172, in addition to the three residues acetylated by YopJ [71]. Lys-172 is located in the catalytic loop of MKKs and serves to coordinate the binding of ATP required for downstream phosphorylation by the activated MKK [71]. VopA thus demonstrates the added ability to inhibit

activated MKKs by preventing the binding of ATP, but not ADP, to the MKK. Finally, the effector VopL (VPA1370) contains three Wiskott –Aldrich homology 2 (WH2) domains interspersed with three proline-rich motifs (PRMs) [34]. WH2 domains have been shown to bind to actin monomers [49] and, in some cases, nucleate actin [24], suggesting that VopL plays a role in manipulation of the actin cytoskeleton. VopL has in fact been shown to nucleate the assembly of actin filaments *in vitro* and in cell culture; moreover, the assembly of actin filaments occurs independent of Arp2/3 or other eukaryotic nucleation factors [34].

Enteropathogenic Models of Infection by *V. parahaemolyticus*

In vivo study of the pathogenesis of *V. parahaemolyticus* has to date relied upon several experimental models, each with distinct shortcomings. The system most commonly used for study of the enteropathogenicity of *V. parahaemolyticus* is the ligated rabbit ileal loop model, wherein the small intestine of an adult rabbit is removed from the abdominal cavity and one or more sections of the ileum are isolated from the remainder of the intestine by ligatures [11, 12]. Experimental preparations are injected into the ligated loops, which are then returned to the abdominal cavity of the rabbit for the duration of the experiment. Following the subsequent sacrifice of the rabbit, the infected loop or loops may be analyzed for fluid accumulation and tissue pathology. Injection of pathogenic strains of *V. parahaemolyticus* into ligated rabbit ileal loops results in dilatation of the loop

due to fluid accumulation, as determined by the ratio of the volume of fluid within the loop to the length of the loop [7]. In a separate study, Park *et al* observed histological changes in infected loop tissue that are consistent with inflammation, including disruption of the villous and epithelial architecture, submucosal edema, and infiltration of the lamina propria by neutrophils (Figure 2) [46]. It is important to note that these latter studies utilized an engineered strain of *V. parahaemolyticus* derived from a pathogenic clinical isolate but lacking any hemolytic activity [46], supporting the notion that TDH and TRH are not the sole determinants of enteropathogenicity in this organism.

Despite the pathology demonstrated by *V. parahaemolyticus* in the rabbit ileal loop model, the closed nature of this system diminishes its physiological relevance. Because the gastrointestinal tract is open and thus exposed to a luminal environment that is in a constant state of flux, actual disease progression likely differs from that modeled in the rabbit ileal loop system. The acute, but generally nonlethal, nature of the inflammatory response induced by *V. parahaemolyticus*

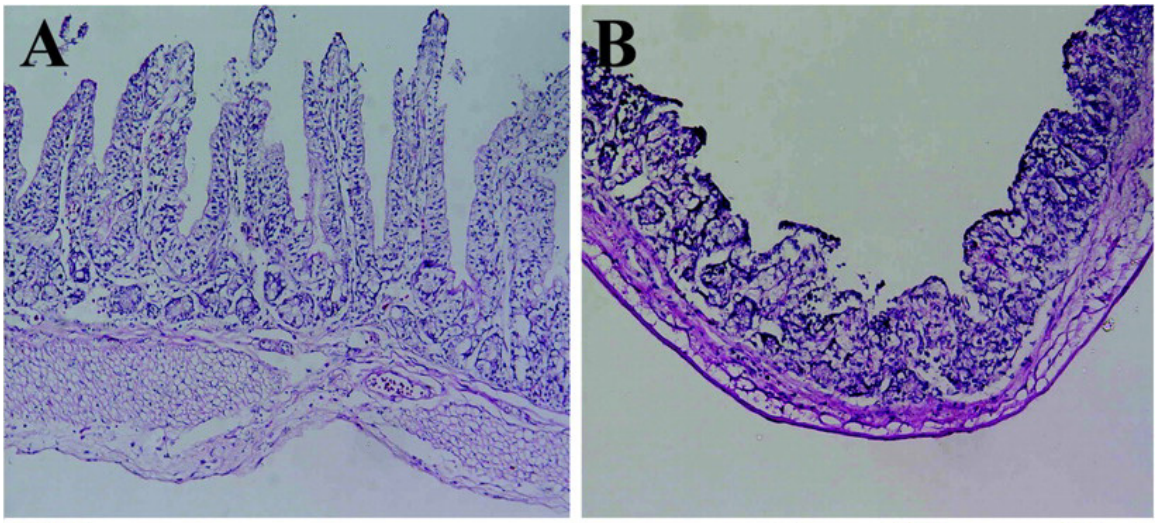

Figure 2. Inflammation induced by *V. parahaemolyticus* in the rabbit ileal loop
Hematoxylin and eosin-stained sections of tissue from ligated rabbit ileal loops infected with (A) PBS and (B) *V. parahaemolyticus* POR1, a RIMD2210633-derived mutant strain that lacks TDH. Modified from [46].

suggests that this pathogen clears the intestinal tract and immune system after a relatively short period of infection. As such, some researchers have utilized models in which the host immune system is not fully developed.One such system, the infant or suckling mouse model, was initially developed for the study of *Vibrio cholerae* [74], though its use has extended to include challenge by *V. parahaemolyticus*. Orogastric infection of infant mice with KP-positive clinical isolates results in increased intestinal fluid accumulation, as measured by the ratio of intestine to body weight [77]. Infection with KP- and TDH-negative, TRH-

positive clinical or environmental strains also induces fluid accumulation, albeit to a lesser extent [77].

Precedence does exist for the infection of adult, wild-type animals with *V. parahaemolyticus*, although such experiments are rare. In 1990, Hoashi and colleagues infected adult mice with various KP-positive and KP-negative strains of *V. parahaemolyticus* isolated from either seafood or infected patients [25]. The LD_{50} was estimated to be ~10^7 colony-forming units (CFU) in mice challenged intraperitoneally and ~10^8 CFU in mice challenged orogastrically, irrespective of the presence or absence of TDH [25]. Infected mice exhibited swelling, redness, and fluid accumulation in the small intestine, which was also found to display marked changes at the histological level, including edema and disruption of the villous architecture (Figure 3) [25]. The ability of TDH-negative strains to induce pathology in infected mice again suggests that one or more additional factors contribute to the enteropathogenicity of *V. parahaemolyticus*. However, induction of an inflammatory response in these animals required infectious doses of *V. parahaemolyticus* near the LD_{50} [25]. That the dose required to induce intestinal inflammation is lethal to half of the mice infected suggests that this model does not accurately replicate *V. parahaemolyticus*-induced gastroenteritis in humans, which carries a much lower mortality rate [82](REF).

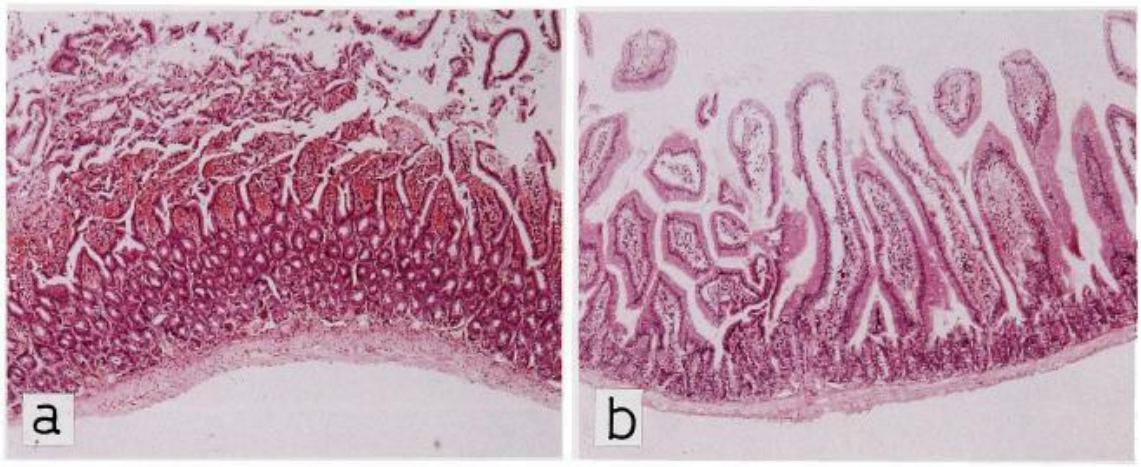

Figure 3. Intestinal inflammation in mice infected with *V. parahaemolyticus*
Hematoxylin and eosin-stained sections of small intestine from mice infected with *V. parahaemolyticus* by (A) intraperitoneal injection or (B) orogastric gavage. Modified from [25].

The Germfree Mouse as a Tool

The shortcomings of the animal models mentioned above highlight the need for a suitable system in which to study the enteropathogenicity of *V. parahaemolyticus*. One alternative that may facilitate the study of the effects of *V. parahaemolyticus* in isolation entails the use of gnotobiotics.

The concept of gnotobiotics is thought to have been first proposed by Louis Pasteur in the late nineteenth century [21, 47], although more than sixty years passed before germfree animals were raised to successive generations by Reyniers and colleagues, who pioneered these studies in rats [53] and chickens [51]. In the 1950s, the first facilities dedicated to the maintenance of germfree rat and mouse colonies were established by Reyniers, at the University of Notre

Dame in the United States, and Gustafsson, at Lund University in Sweden [21]. While at present the chicken, rat, and mouse remain the organisms most widely used for gnotobiotic experimentation, germfree systems have been established and are in use for a number of other animals, including the guinea pig, rabbit, dog, and pig.

The most widely used terminology pertaining to the field of gnotobiology was put forth by Reyniers in 1949 [52], though no system is universally accepted. The term *gnotobiotic* is derived from the Greek *gnotos* ("known") and *biota* ("life"). In this document, the term *gnotobiote* will be used in reference to any animal born aseptically, housed in sterile isolator conditions, and whose associated microbial composition is explicitly defined. *Germfree* will be used to define those animals shown to be demonstrably void of any form of associated life, while the term *ex-germfree* will be used in reference to animals maintained in a germfree state until the introduction of external microbes, known or otherwise. Animals raised under ordinary conditions (i.e., not germfree) are referred to as *conventional*, while *conventionalized* refers to ex-germfree animals that have been exposed to the microbiota of a conventional control animal.

The isolation of germfree animals in a sterile environment results in distinct anatomical and physiological differences in relation to their conventionally raised counterparts. In the mouse, some of the most pronounced differences are observed in the gastrointestinal tract. The cecum is notably

enlarged in relation to that of a conventionally raised mouse, with contents measuring an average of 6-10% and, in some cases, nearly 25% of body weight (Figure 4) [20]. The size discrepancy was subsequently found to result from an accumulation of mucus that is typically degraded by microbes residing in the cecum [80]. The mucus is composed of negatively charged glycoproteins that attract water molecules to the cecum and also retard sodium-dependent transport of water out of the cecum [3, 22]. The germfree cecum can be reduced to conventional proportions upon inoculation of the germfree animal with the cecal contents of a conventionally raised animal [65]. The morphological differences in the cecum also suggest functional differences, as removal of the cecum restores the metabolic rate, which is lowered in germfree animals, to conventional levels [8].

Isolation in a germfree environment would also be expected to impact development and function of the immune system, and changes in the composition of gut-associated lymphoid tissue (GALT) have indeed been observed in colonization studies utilizing germfree mice. Conventionalization of germfree mice results in expansion of T-cell receptor (TCR)-positive intraepitheliar lymphocytes (IELs) [1, 76].

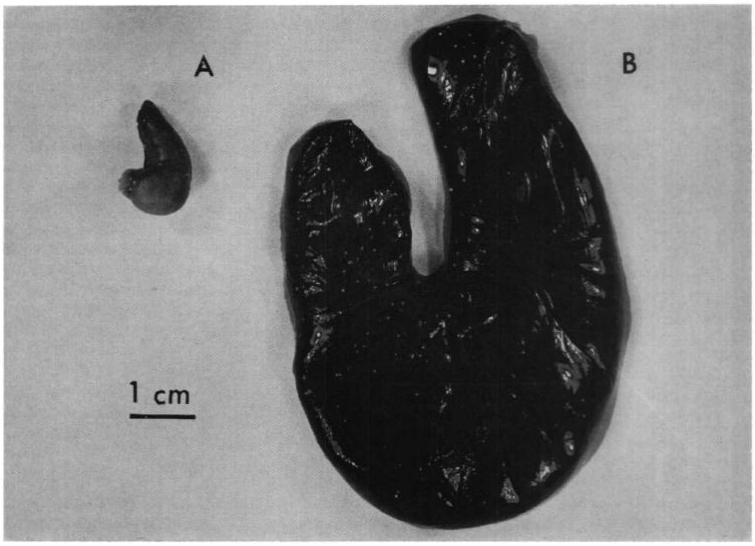

Figure 4. The cecum is enlarged in germfree mice
Representative ceca from isogenic, conventionally raised (A) and germfree (B) mice are shown. Modified from [20].

One of the most useful aspects of gnotobiotic experimentation is the ability to characterize the specific effects of colonization by a single bacterial species. To that end, a number of systems involving colonization by both nonpathogenic and pathogenic bacteria are well established. For example, the commensal bacterium *Bacteroides thetaiotaomicron* has been shown to possess the capability to initiate a program of changes in intestinal gene expression associated with conventionalization. Among the genes upregulated are those involved in lipid and nutrient absorption, intestinal motility, and strengthening of the intestinal epithelial barrier [29]. Fortification of the mucosal barrier safeguards the intestine against invasion by intestinal bacteria, and colonization

with *B. thetaiotaomicron* does not induce an inflammatory immune response. On the other hand, oral infection of germfree mice with the pathogen *Salmonella typhimurium* results in colitis characterized by edema, infiltration by neutrophils, crypt abscesses, and disruption of the epithelial cell layer [66]. This pathology is similar to that described in documented cases of *S. typhimurium* infection in humans [6], as well as cattle [59].

Objectives

Study of the enteropathogenic process induced by infection with *V. parahaemolyticus* has been hampered by the lack of a practical and physiologically relevant animal model. Thus, the goal of this study is to develop a system of *V. parahaemolyticus*-induced enteropathogenicity in the germfree mouse. The model will be evaluated using a number of parameters, most notably colonization of the mouse intestine and inflammation of intestinal tissues. Additionally, the relative contributions of TDH, T3SS1, and T3SS2 to enteropathogenicity will be determined with the use of mutants lacking one or more of these components. The establishment of a physiologically relevant, tractable *in vivo* model of *V. parahaemolyticus*-associated gastroenteritis will provide a valuable tool for future study of the virulence of this pathogen.

CHAPTER TWO
Materials and Methods

Bacterial Strains and Culture

V. parahaemolyticus RIMD2210633, POR1, POR2, and POR3 (gifts of T. Honda) were streaked onto marine Luria Bertani (MLB) agar plates (1% tryptone, 0.5% yeast extract, 3% NaCl, and 1.5% Bacto agar per liter) and incubated at 30° C overnight, followed by room temperature (25° C) benchtop incubation for at least 72h. Single bacterial colonies were cultured overnight at 30° C with shaking in Heart Infusion (HI) medium (Becton-Dickinson). Prior to gavage, overnight cultures were diluted to 0.5 OD in HI medium and incubated at 37° C with shaking for 90 minutes to induce the T3SS. Cultures were centrifuged and resuspended in sterile phosphate-buffered saline (PBS) at a concentration of 2 x 10^{10} CFU/ml.

Germfree Mouse Maintenance

Wild-type FVB/nCr2Tox176 mice were obtained from the laboratory of Lora Hooper in the Center for Immunology at UT Southwestern. Mice were housed in flexible film isolators assembled using components from Class Biologically Clean (location) and Standard Safety Equipment (location). The air supply in each isolator was controlled by a motor blowing air through a sterilizing

intake filter. Each isolator was used to house up to 10 cages containing up to 4 mice each. Mice were fed autoclaved, irradiated chow (Purina) and were removed from isolators 1-2 hours prior to the start of the experiment.

Mouse Infection

Using a 1-milliliter syringe attached to a blunt-tipped metal gavage needle, mice between 8 and 24 weeks of age were orally gavaged with 10^9 CFU of *V. parahaemolyticus* (see above) in a volume of 100 µl sterile PBS, or with 100 µl of PBS alone as a control. The syringe and needle were flushed with 70% ethanol, sterile dH_2O, and sterile PBS prior to administration of each strain. Cages housing no more than 3 mice each were maintained in a sterile hood during the course of infection. Infected mice were sacrificed 24 to 48 hours following infection by intraperitoneal injection of 50 µl Euthasol (Virbac), followed by cervical dislocation. The weight of each mouse was recorded both prior to infection and upon sacrifice.

Mouse Dissection and Sample Collection

Following sacrifice, mice were dissected using tools sterilized by immersion in 70% ethanol and subsequent passage through a Bunsen burner flame. The mouse was pinned to a Styrofoam board, doused with 70% ethanol, and the abdomen was opened using a vertical incision down the midline.

Horizontal incisions made at the top and bottom of the initial incision created two flaps of skin, which were peeled away from the mouse. Following resterilization of the dissection tools, a second, identical set of incisions was made through the peritoneum to expose the body cavity.

Sterilized dissecting scissors were used to sever the gastrointestinal tract at the junction between the stomach and small intestine. The small intestine was subsequently removed from the abdominal cavity and placed in a sterile Petri dish, after which a cut was made at the ileocecal junction to separate the small intestine from the large intestine. An incision was made between the distal portion of the descending colon and the rectum to separate the large intestine, which was removed from the abdominal cavity to a sterile Petri dish. Instruments were resterilized and an incision was made between the colon and cecum to separate the two organs. Using flame-sterilized instruments, a 1-cm length of the proximal end of the colon was collected for subsequent freezing and RNA processing (see following sections). A sterile plastic 1 μl inoculating loop (Nunc) was inserted into the proximal end of the remaining colon for collection of a luminal sample, which was resuspended in 1 ml sterile PBS in a sterile microcentrifuge tube and placed on ice prior to dilution plating (see Bacterial Dilution Plating and Enumeration). Instruments were again resterilized and a small incision was made in the center of the cecum. A 1 μl sample of the cecal lumen was collected by insertion of a sterile plastic inoculating loop through the

incision. This sample was also resuspended in 1 ml sterile PBS and placed on ice in preparation for dilution plating. Forceps and dissecting scissors were used to separate and remove fat within the abdominal cavity, including fatty tissue associated with the intestines prior to their removal. The collected tissue was placed in 3 ml sterile PBS in a 14-ml Falcon tube and placed on ice in preparation for dilution plating of mesenteric lymph nodes (MLN). Finally, the spleen was carefully removed from the abdominal cavity using forceps and also placed on ice in 3 ml sterile PBS.

Tissue Preparation and Fixation

Small intestine—Following removal of the small intestine to a sterile Petri dish during dissection, a 1-cm section of ileum was removed from the distal end and discarded to ensure that no cecal tissue was present in the ileal sample. A 2-cm section was subsequently collected from the distal end of the ileum, and a syringe fitted with a blunt plastic-tipped gavage needle was used to flush the lumen with sterile PBS. The rinsed tissue was then cut in half and each piece was placed into a separate, sterile 1.5-ml microcentrifuge tube. Tissue samples were snap frozen in liquid nitrogen and stored at -80° C for isolation of RNA at a later date.

Colon—Prior to sampling of the luminal contents (detailed in previous section), a 1-cm section of the proximal end of each colon was flushed with PBS and placed in a 1.5-ml microcentrifuge tube, snap-frozen in liquid nitrogen, and stored at -80°

C for purification of RNA at a later date. Following collection of the luminal sample, the remaining colon tissue was slit longitudinally and pinned flat onto a wax plate (Carolina Biological) lumen side up. The tissues were bathed in Bouin's fixative (Ricca Chemical) for 24h at 4° C, followed by a brief rinse with deionized tap water and 3 successive overnight washes in 70% ethanol. Samples were subsequently rolled into a "Swiss roll" preparation and dipped in molten 2% agarose (Fisher) dissolved in H_2O to maintain the shape of the roll.

Cecum—Following collection of a luminal sample from the cecum, the tissue was cut in half and both halves flushed thoroughly with sterile PBS to remove intestinal contents. One half of the rinsed cecum was again cut in half and each resulting section was placed in a sterile 1.5-ml microcentrifuge tube, snap frozen, and stored at -80° C for purification of RNA at a later date. The remaining half of the cecum was placed in 50-ml conical vial containing 5 ml Bouin's fixative and fixed as described for colon samples.

Bacterial Dilution Plating and Enumeration

Luminal samples from the colon and cecum were previously diluted 1000-fold, or 10^{-3}, in PBS (see Mouse Dissection and Sample Collection). From these dilutions, four successive serial tenfold dilutions were made in PBS to yield dilutions ranging from 10^{-4} to 10^{-7}. 100 µl of each of the 10^{-4} through 10^{-7} dilutions was plated, using sterile glass beads, onto minimal marine media

(MMM) agar plates (5 mM K_2SO_4, 77 mM K_2HPO_4, 35 mM KH_2PO_4, 20 mM NH_4Cl, 5 mM $MgSO_4 \cdot 7H_20$, 2% NaCl, 0.4 % galactose, and 1.5% Bacto agar per liter) supplemented with 0.1% sodium pyruvate. Final dilutions of the plated samples were 10^{-5}, 10^{-6}, 10^{-7}, and 10^{-8}. Plates were incubated at 30° C for 48 hours.

Spleen and MLN were previously collected from each animal and stored on ice in 3 ml sterile PBS per sample (see Mouse Dissection and Sample Collection). Each sample, including PBS, was homogenized using an Omni TH homogenizer fitted with an autoclaved, hard tissue probe for ~30 seconds. Between samples, the probe was rinsed in 70% ethanol followed by PBS. The resulting homogenate was used to make two successive serial tenfold dilutions in sterile PBS. 100 µl of the homogenate and dilutions were each plated onto MMM agar plates supplemented with 0.1% sodium pyruvate. Plates were incubated at 30° C for 48 hours.

Following incubation, bacteria were enumerated by counting the number of colonies on each plate. The number of colony-forming units (CFU) per milliliter of luminal content was calculated by multiplying the number of colonies per plate by the dilution factor of the plate. For spleen and MLN, the same procedure was used to calculate CFU per organ. Where possible, only plates containing greater than 100 colonies were used in calculating CFU. Data were

compiled in Microsoft Excel and graphs were generated using Prism 5 (GraphPad).

Slide Preparation

Fixed tissue samples were submitted to the Molecular Pathology Core Facility at UT Southwestern for paraffin processing, embedding, and sectioning following established protocols [62, 79].

Hematoxylin and Eosin Staining

Hematoxylin and eosin staining of paraffin-embedded tissue sections was performed by the Molecular Pathology Core Facility at UT Southwestern using a DRS-601 X-Y-Z robotic stainer (Sakura) and commercially prepared solutions and following established protocols [62, 79].

RNA Isolation and cDNA Synthesis

RNA isolation—Following removal from storage at -80° C, all tissues were kept on dry ice until immediately before processing. An Omni TH homogenizer was used to homogenize snap-frozen colon and cecal tissues in Qiagen Buffer RLT (from the RNeasy Midi RNA isolation kit) and β-mercaptoethanol (Bio-Rad). Prior to use, the homogenizer probe was rinsed in 0.1 M NaOH, 1 mM EDTA followed by RNase-free water to invactivate any RNases. Each sample was

homogenized for 30 seconds, and the homogenizer probe was rinsed three times successively in RNase-free 70% ethanol and once in RNase-free H_2O between each sample. RNA was isolated from lysates using the reagents and protocol from the RNeasy Midi kit. RNA was eluted in 150 µl RNase-free H_2O and quantitated by measuring absorbance, at 260 and 280 nm, of a 1:50 dilution of RNA in 10mM Tris-HCl, pH 7.5. RNA was stored at -20° C or -80° C prior to treatment with DNase.

DNase treatment—10 µg of isolated RNA was treated with RNase-free DNase (Roche) at a final concentration of 0.2 U DNase per µg RNA, in a 100-µl reaction that also included 10 mM $MgCl_2$, 1 mM dithiothreitol (DTT), and 1 unit RNase OUT (Invitrogen). RNA was incubated with DNase in a 37° C water bath for 15 minutes and subsequently purified using the reagents and protocol from the Qiagen RNeasy Mini kit. At the end of purification, RNA was eluted in 30 µl RNase-free H_2O and quantitated as previously detailed. Purified, DNase-treated RNA was stored at -20°C prior to cDNA synthesis.

cDNA synthesis—All samples, reagents, and master mixes were maintained on ice during reaction assembly. 2 µg DNase-treated RNA was used as a template for cDNA synthesis. RNA was incubated with 250 ng random hexamers (Invitrogen) at 65° C for 5 minutes in a nuclease-free PCR tube, which was then placed immediately on ice. 2 µl of each RNA-hexamer mixture was reserved for use as a

negative control in a separate PCR tube. A reverse transcriptase master mix was subsequently added to each sample to yield an 18-µl reaction containing 10 mM DTT (Sigma, Invitrogen), 1 mM dTNPs (Invitrogen), 6 units RNase OUT (Invitrogen), and 200 units Moloney Murine Leukemia Virus (M-MLV) Reverse Transcriptase (Invitrogen). For negative control samples, a separate master mix was assembled that lacked reverse transcriptase but in which the concentrations of all other reagents remained unchanged. 2 µl of this master mix was added to each negative control RNA sample. All samples were then incubated at 25° C for 10 minutes, 42° C for 1 hour, and chilled to 4° C in a thermal cycler (Bio-Rad).

Upon completion of cDNA synthesis, the reaction mixture was diluted in RNase-free H_2O to a final volume of 200 µl. Negative control reactions were diluted to a final volume of 12 µl. 2 µl cDNA was used in a PCR reaction to check for contamination by genomic DNA, using primers spanning an intron-exon boundary of mouse actin. Primers used for amplification of actin were synthesized by Integrated DNA Technologies and are as follows: 5'-GAA GTA CCC CAT TGA ACA TGG C, 3'-GAC ACC GTC CCC AGA ATC C. Each PCR reaction had a final volume of 25 µl and consisted of 0.5 µM forward primer, 0.5 µM reverse primer, 1X PCR buffer (-)Mg (Roche), 2.5 mM $MgCl_2$ (Invitrogen, Sigma), 0.2 mM dNTPs, and 0.625 units Taq polymerase (Roche). Samples were amplified through 35 cycles with an annealing temperature of 58°

C and an extension time of 1 minute per cycle. Reaction products were visualized by electrophoresis through a 3% agarose gel.

Quantitative RT-PCR

For each qRT-PCR reaction, 2 μl cDNA was added to a 25 μl reaction mixture containing 1X Platinum SYBR Green qPCR Supermix (Invitrogen) and 300 nM each forward and reverse primer. Each reaction was run in triplicate using a Stratagene Mx3000P QPCR system. Primers used for amplification are as follows: IL-1β forward 5'-TGG TAC ATC AGC ACC TCA CAA GCA-3', IL-1β reverse 5'-AGG CAT TAG AAA CAG TCC AGC CCA-3'; CXCL9 forward 5'-TCA GAT CTG GGC AAG TGT CCC TTT-3', CXCL9 reverse 5'-TGA GGT CTA TCT AGC TCA CCA GCA-3'; 18S forward 5'-CAT TCG AAC GTC TGC CCT ATC, 18S reverse 5'-CCT GCT GCC TTC CTT GGA-3'

Immunohistochemistry

Slides containing unstained, paraffin-embedded tissue samples were prepared by the UTSW Molecular Pathology Core Facility (see Slide Preparation). Slides were deparaffinized in 2 successive 5-minute washes in xylene, followed by a series of 3-minute washes in graded ethanol (100%, 100%, 95%, 70%) and a 10-minute rinse under running tap water. Endogenous peroxidase activity was blocked by incubation at room temperature in 30%

hydrogen peroxide diluted 1:10 in 1X PBS (Sigma). Antigen retrieval was performed by incubating in a freshly made buffer containing 10 mM sodium citrate, 0.05% Tween 20, pH 6.0 at 98° C for 15 minutes. Following a 5-minute wash in 1X PBS, slides were blocked in Blocking Buffer 1 (1X PBS, 2% BSA) for 15 minutes, washed in 1X PBS for 5 minutes, and blocked in Blocking Buffer 2 (1X PBS, 1% BSA, 0.3% Triton X-100) for an additional 15 minutes to permeabilize cell membranes. Slides were incubated with prediluted rabbit polyclonal anti-myeloperoxidase primary antibody (Abcam) overnight at 4° C in a humid chamber. Slides were subsequently washed in three successive 5-minute washes in 1X TBS plus 0.1% Tween (TBS-T) and incubated with biotinylated α-rabbit secondary antibody (Vector Labs) diluted 1:500 in Blocking Buffer 1 for 30 minutes at room temperature. Following three more successive 5-minute washes in 1X TBS-T, signal was amplified for 30 minutes at room temperature using ABC reagent (Vector Labs). Immunoperoxidase labeling was detected with diaminobenzidine (DAB) (Vector Labs), followed by counterstaining with Harris' hematoxylin (Sigma) and a 10-minute rinse under running tap water. Slides were then washed for 5 minutes in 1X TBS-T and dehydrated with a series of 3-minute washes in graded ethanol (70%, 95%, 100%, 100%) followed by two successive 5-minute washes in xylene. Coverslips were mounted with Cytoseal (Richard-Allan Scientific) and allowed to air dry before microscopic examination.

Immunofluorescence

Slides containing unstained, paraffin-embedded tissue samples were prepared by the UTSW Molecular Pathology Core Facility (see Slide Preparation). Slides were deparaffinized in 2 successive 5-minute washes in xylene, followed by a series of 3-minute washes in graded ethanol (100%, 100%, 95%, 70%) and a 10-minute rinse under running tap water. Antigen retrieval was performed by incubating in a freshly made buffer containing 10 mM sodium citrate, 0.05% Tween 20, pH 6.0 at 98° C for 20 minutes. Following a 5-minute wash in 1X PBS, slides were blocked in Blocking Buffer 1 for 15 minutes, washed in 1X PBS for 5 minutes, and blocked in Blocking Buffer 2 for an additional 15 minutes to permeabilize cell membranes. Slides were incubated with rabbit polyclonal anti-Ki67 primary antibody (Abcam), diluted 1:1000 in Blocking Buffer 1, overnight at 4° C in a humid chamber. Slides were subsequently washed in three successive 5-minute washes in TBS-T and incubated with biotinylated α-rabbit secondary antibody (Vector Labs) diluted 1:500 in Blocking Buffer 1 for 30 minutes at room temperature. Following three more successive 5-minute washes in 1X TBS-T, signal was amplified for 30 minutes in the dark at room temperature using 2 mg/ml Alexa Fluor 594-conjugated streptavidin diluted 1:500 in Blocking Buffer A. Slides were washed 3 times successively in 1X TBS-T in a light-protected chamber. To stain nuclei, slides were incubated with Hoechst (Sigma) diluted 1:5000 in Blocking Buffer A for 15 minutes in the dark at room temperature.

Slides were washed once in 1X TBS-T for 5 minutes. Coverslips were mounted with 1X PBS plus 10% glyercol plus *N*-propyl gallate, sealed with clear nail enamel (Revlon), and allowed to air dry before microscopic examination. Slides were stored for up to 2 weeks in a light-protected box at 4° C.

Microscopy

Light microscopy—A Leica DM2000 photomicroscope equipped with brightfield illumination was used. Digital micrographs were captured using an Optronics Microfire digital CCD color camera in conjunction with an Apple Macintosh G4 computer running PictureFrame 2 image acquisition software (Optronics). Images were processed using Adobe Photoshop CS2.

Fluorescence microscopy—A Zeiss Axiovert 200 microscope equipped with epifluorescence was used. Digital micrographs were captured using a Hamamatsu Orca-ER camera in conjunction with an Apple Macintosh G4 computer running OpenLab 3.5.1 imaging software (Improvision). Images were colored using OpenLab 3.5.1 and processed using Adobe Photoshop CS2.

CHAPTER THREE
Results

Colonization of the Mouse Intestine by *V. parahaemolyticus*

The initial step in developing a mouse model of infection by *V. parahaemolyticus* was to evaluate the ability of *V. parahaemolyticus* to colonize the intestine of infected mice. To this end, conventionally raised and germfree wild-type mice were administered 10^9 CFU of *V. parahaemolyticus* RIMD2210633 by orogastric gavage. Mice were infected for 48 hours and subsequently sacrificed for sample collection. Intestinal colonization by *V. parahaemolyticus* was determined by enumerating bacteria cultured from the luminal contents of the cecum and colon. As shown in Figure 5, we were unable to recover *V. parahaemolyticus* from either the cecum (panel A, left column) or colon (panel B, left column) of conventionally raised, infected mice. However, these bacteria were recovered on the order of ~10^9 CFU/ml from the lumen of the cecum (panel A, right column) and colon (panel B, right column) of germfree infected mice. These results suggested that colonization resistance, a well-documented phenomonenon in which intestinal microbiota inhibit the proliferation of potential pathogens [78], plays a role in preventing *V. parahaemolyticus* from establishing residence in the conventially raised mouse

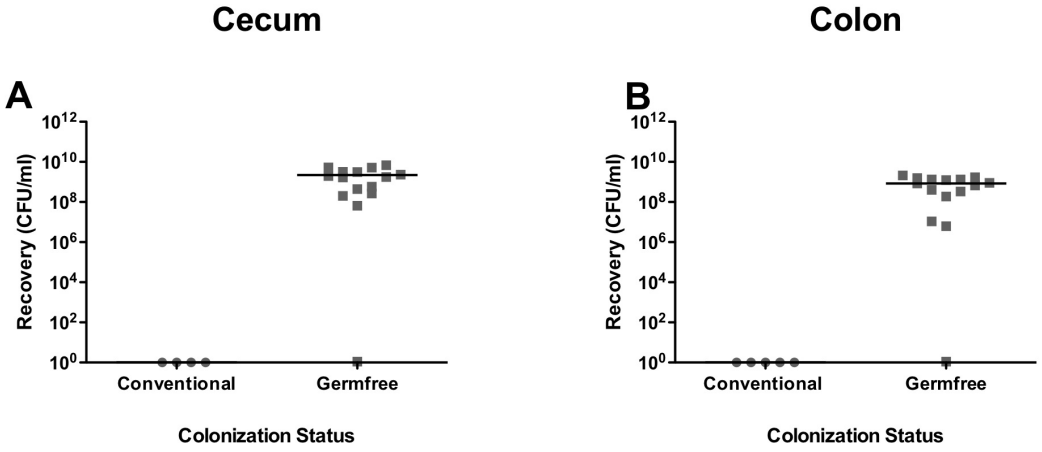

Figure 5. *V. parahaemolyticus* colonizes the intestine of germfree but not conventionally raised mice
Conventionally raised and germfree mice were infected for 48 hours with *V. parahaemolyticus* RIMD2210633 Bacteria were cultured from lumen of the cecum (A) and colon (B) of infected mice and enumerated by dilution plating.

intestine. As a consequence, only germfree mice were used in all subsequent experiments

We next sought to determine whether TDH, T3SS1, or T3SS2 impacted the ability of *V. parahaemolyticus* to colonize the mouse intestine. In order to do so, we utilized a number of mutant strains, derived from the clinical isolate RIMD2210633, that lack these components. The mutant strains used will be referred to collectively as the POR strains and are identified as POR1, POR2, and POR3. POR1 contains a deletion of the *tdhA* and *tdhS* genes that encode TDH and thus lacks both TDH and TRH [45]. Both POR2 and POR3 are derived from

the POR1 strain and therefore are also TDH- and TRH- negative. Additionally, POR2 carries an inactivating mutation in the *vcrD1* gene, which encodes a structural component of T3SS1 [46]. Inactivation of *vcrD1* therefore prevents the translocation of effectors through T3SS1, so that in the POR2 strain effectors are only secreted from T3SS2. Likewise, POR3 carries an inactivating mutation in the *vcrD2* gene, which encodes a structural component of T3SS2, and in this strain effectors are only secreted from T3SS1 [45].

Germfree mice were infected for 24 (Fig. 6, A-B) or 48 (Fig. 6, C-D) hours with POR1, POR2, or POR3. All three mutant strains were recovered from the cecum (left panels) and colon (right panels) at a level similar to the recovery of RIMD2210633, ~10^9 CFU/ml. These data suggest that colonization of the lower germfree mouse intestine by *V. parahaemolyticus* occurs within 24 hours and is independent of TDH, T3SS1, and T3SS2.

As mentioned earlier, the human diseases caused by *V. parahaemolyticus* are dependent on the route of infection taken by the bacterium. While septicemia commonly occurs as a result of a wound infection, diarrhea and other symptoms of gastroenteritis are more likely to develop from oral infection. We thus reasoned that the oral gavage mode of infection used in these experiments would result in pathology that remains localized to the intestine and examined the mesenteric lymph nodes (MLN) and spleen of infected mice for the presence of *V.*

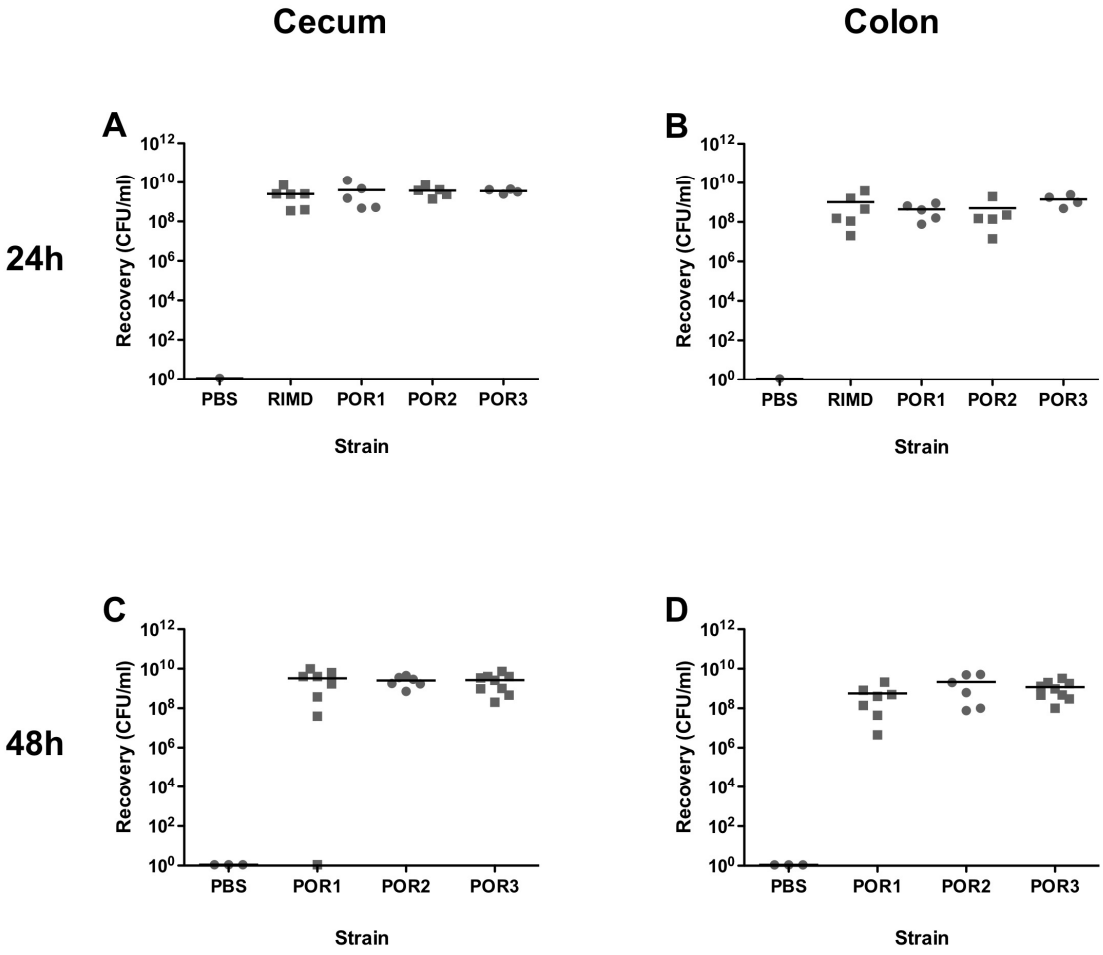

Figure 6. *V. parahaemolyticus* RIMD2210633 and POR strains colonize the intestine of germfree mice

Germfree mice were infected for 24 (A-B) or 48 (C-D) hours with PBS or *V. parahaemolyticus* RIMD2210633, POR1, POR2, or POR3 Bacteria were cultured from lumen of the cecum (left panels) and colon (right panels) of infected mice and enumerated by dilution plating.

parahaemolyticus; the recovery of bacteria from these tissues would suggest systemic spread of the infection beyond the gastrointestinal tract. After 24 hours, bacterial recovery from the MLN (Fig. 7A) and spleen (Fig. 7B) of nearly all infected mice was below the reliable level of detection of our assay (represented in Figure 7 as a dotted line). However, ~10^4 and ~10^3 CFU of RIMD2210633 were recovered from MLN and spleen, respectively, of three of the seven mice infected with this strain at 24 hours. 48 hours post infection, the number of bacteria recovered from both the MLN (Fig. 7A) and spleen (Fig. 7B) were below the reliable level of detection of the assay in nearly all mice. The recovery of bacteria from the MLN, but not the spleen, suggests that limited numbers of bacteria are translocated from the intestinal lumen to the mesentery but do not induce sepsis.

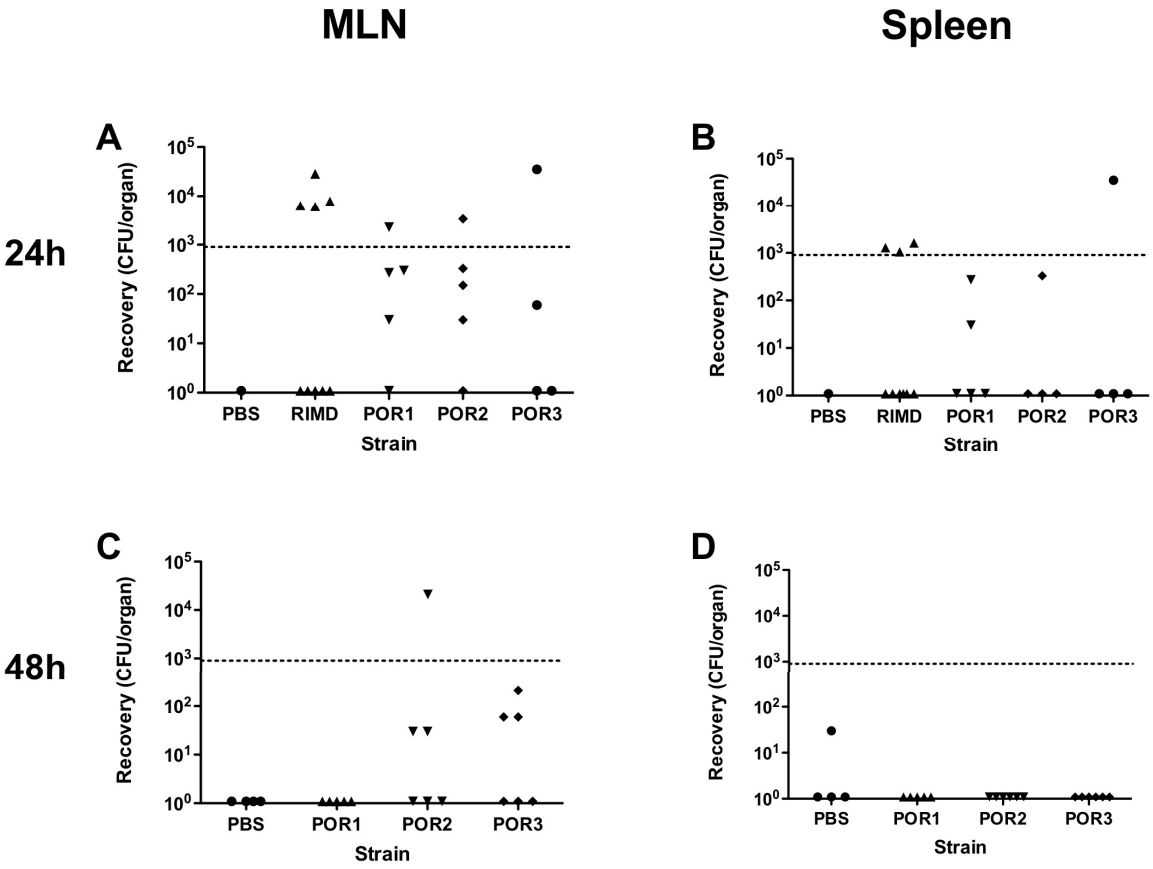

Figure 7. ***V. parahaemolyticus*** **is not recovered from the lymph or spleen of infected germfree mice**

Bacteria were cultured from the mesenteric lymph nodes and spleen of germfree mice infected for (A-B) 48 or (C-D) 24 hours with *V. parahaemolyticus* RIMD2210633, POR1, POR2, or POR3 and enumerated by dilution plating.

***V. parahaemolyticus*-induced intestinal inflammation**

Upon establishing the ability of *V. parahaemolyticus* to colonize the germfree mouse intestine, we turned our focus to the host response to infection. Because oral infection by *V. parahaemolyticus* is largely localized to the gastrointestinal tract, we analyzed hematoxylin and eosin-stained sections of intestinal tissues for pathology. As a control, germfree mice were infected for 24 or 48 hours with sterile PBS. The architecture of the cecum in these mice (Fig. 8, A-B) is organized into epithelium, mucosa, submucosa, and muscularis. The mucosa is further organized into individual crypts that are surrounded by lamina propria. At both 24 and 48 hours, the histology of the cecum appears normal in PBS-infected mice. Infection with RIMD2210633 results in a number of morphological changes to the cecum at both 24 and 48 hours (Fig. 8C and 8D, respectively), including damage to the epithelium, crypt abscess and hyperplasia, expansion of the submucosa by edema fluid, and infiltration of the submucosa and lamina propria by neutrophils. An expanded view of the RIMD2210633-infected cecum is depicted in Figure 4 so that the extent of expansion and hyperplasia may be fully appreciated.

To delineate the role of TDH and the two T3SSs in *V. parahaemolyticus*-induced cecal inflammation, we infected mice with the RIMD2210633-derived POR strains. Infection with POR1, which lacks TDH but contains both a functional T3SS1 and T3SS2, results in a phenotype similar to that of RIMD2210633 but to

a somewhat lesser extent. While crypt abscess and hyperplasia, submucosal expansion, and neutrophil infiltration are all observed at 24 hours (Fig. 8E), by 48 hours much of the pathology has been resolved (Fig. 8F). In the ceca of mice infected with POR2, which lacks both TDH and a functional T3SS1 but does possess a functional T3SS2, the inflammatory phenotype at 24 hours is nearly as severe as that of RIMD2210633 (Fig. 8G). However, at 48 hours inflammation is again largely resolved and the remaining pathology is limited to crypt hyperplasia and a slight thickening of the submucosa (Fig. 8H). Infection with POR3, which lacks TDH and a functional T3SS2 but possesses a functional T3SS1, results in an attenuated inflammatory phenotype. While crypts from the ceca of POR3-infected mice appear slightly elongated at 24 hours (Fig. 8I), at 48 hours the cecum appears identical to the PBS control (Fig. 8J). Taken together, these data suggest that inflammation of the cecum is T3SS2-dependent and T3SS1-independent, while the duration of damage due to infection is associated with the presence of TDH.

In our analysis of the effects of *V. parahaemolyticus* infection on the intestine, we also examined histological samples of colon tissues obtained from infected mice. The architecture of PBS-infected colon tissue is similar to that of the cecum, although crypts are slightly longer in the colon than in the cecum (Fig. 10A). While infection with *V. parahaemolyticus* RIMD2210633 for 48 hours appears to induce an inflammatory response characterized primarily by

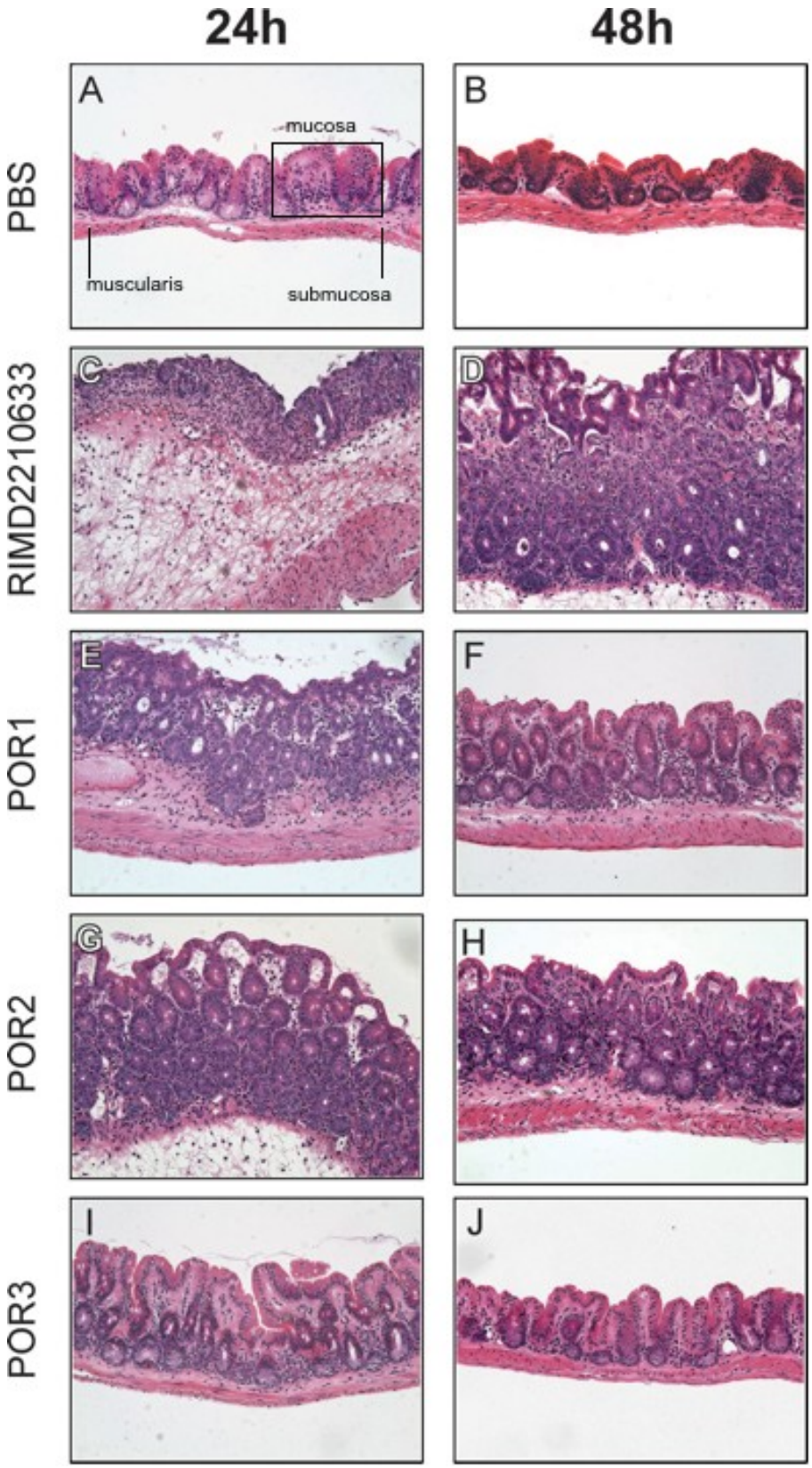
24h
48h
PBS
RIMD2210633
POR1
POR2
POR3
A
B
C
D
E
F
G
H
I
J
mucosa
muscularis
submucosa

submucosal expansion (Fig. 10B), the severity of inflammation is greatly decreased relative to the cecum at this timepoint. Moreover, infection with POR1, POR2, or POR3 results in a histological phenotype that appears similar to the PBS control (Fig. 10, C-E), suggesting that the colon is less affected than the cecum by infection with *V. parahaemolyticus*. Additional analysis also suggested that the small intestine appeared unaffected by infection with *V. parahaemolyticus* (data not shown). For this reason, we highlighted the cecum as the focus of the remaining histological analysis.

Figure 8. *V. parahaemolyticus* infection induces T3SS2-dependent inflammation in the cecum of germfree mice (previous page)
Ceca were isolated from germfree mice infected for 24 hours (left column) or 48 hours (right column) with (A-B) PBS, (C-D) RIMD2210633, (E-F) POR1, (G-H) POR2, or (I-J) POR3. Tissues were fixed, paraffin embedded, and stained with hematoxylin and eosin. Arrows denote representative areas of crypt ulceration. All images are magnified 20X.

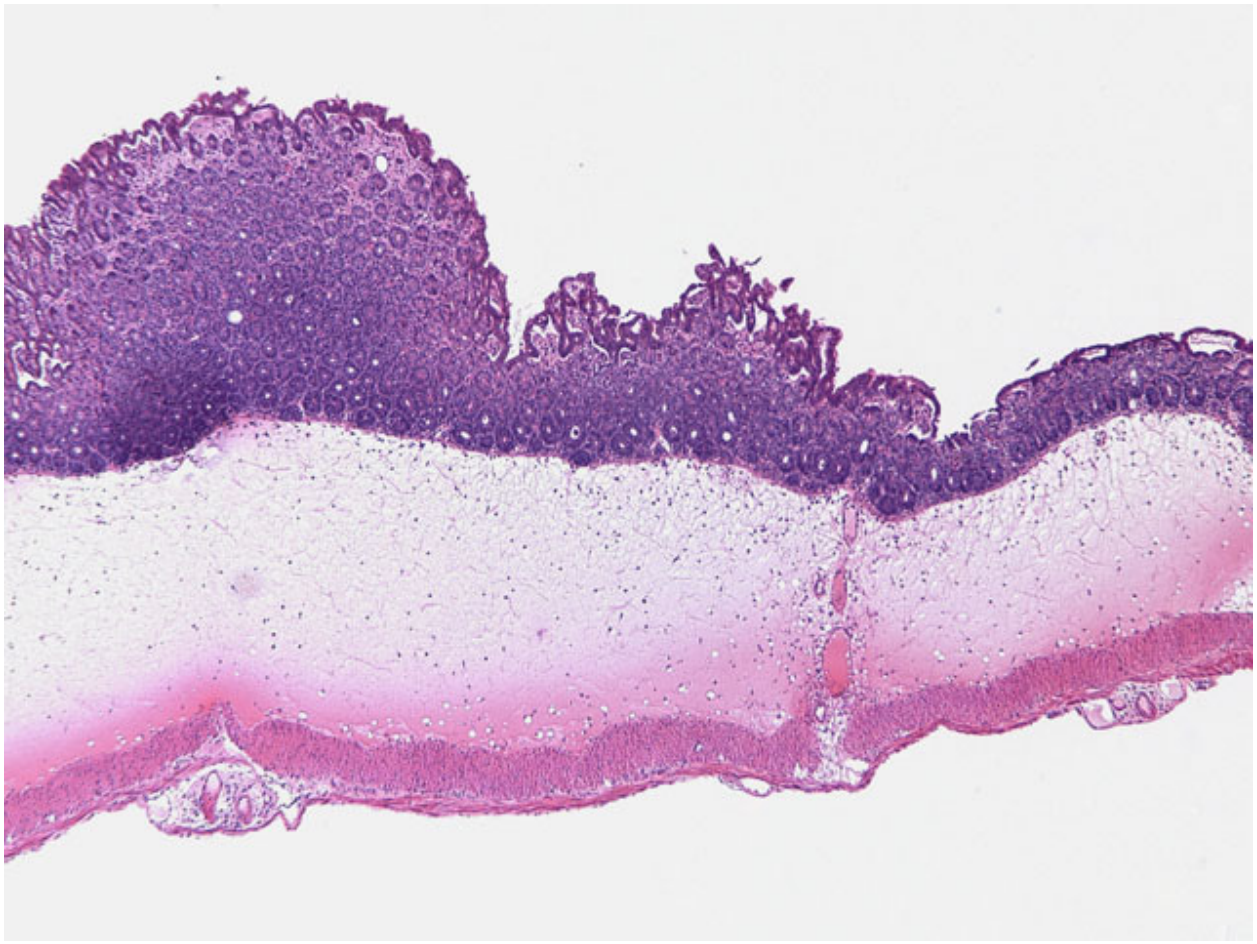

Figure 9. Expanded view of the cecum of a RIMD2210633-infected germfree mouse
Box indicates area depicted in Fig. 9D. Image is magnified 4X.

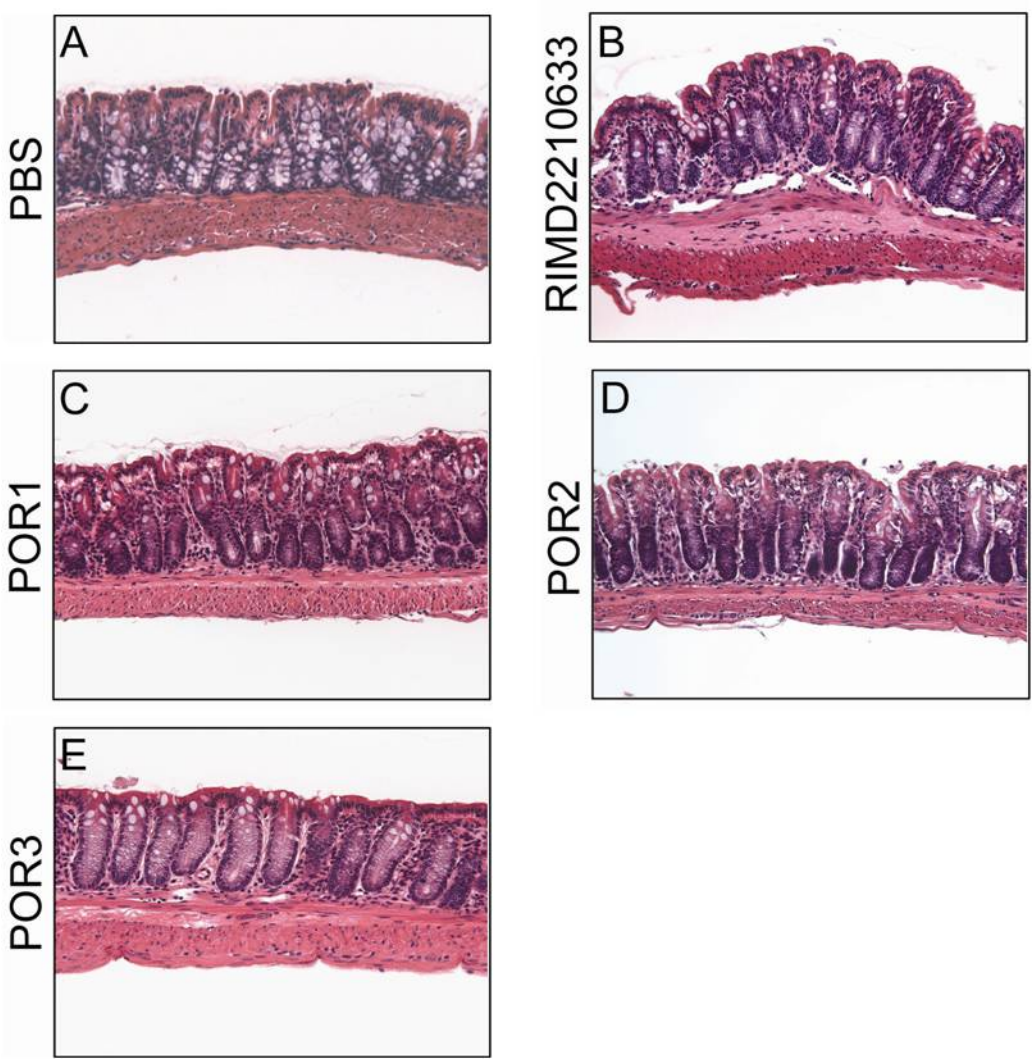

Figure 10. ***V. parahaemolyticus*** **RIMD2210633 induces slight inflammation in the colon of germfree mice**

Colons were isolated from germfree mice infected for 48h with (A-B) PBS, (C-D) RIMD2210633, (E-F) POR1, (G-H) POR2, or (I-J) POR3. Tissues were fixed, paraffin embedded, and stained with hematoxylin and eosin. All images are magnified 20X.

Hematoxylin and eosin-stained sections of cecal tissue appeared to reveal an influx of neutrophils into the mucosa and submucosa. To confirm the identity of these cells, we stained paraffin-embedded sections of cecum with an antibody against myeloperoxidase (MPO), an enzyme commonly used as a marker of neutrophils. In PBS-infected control tissues, neutrophils are present and localized primarily to the epithelium (Fig. 11A). When mice were infected with RIMD2210633 for 48 hours, neutrophils localized to the lamina propria and expanded submucosa of the cecum (Fig. 11B). Fewer neutrophils localized to the epithelium than in the control sample, which may perhaps be attributed to disruption of the epithelial layer during infection. In mice infected with POR1, neutrophils again localized to the epithelial layer, as well as the submucosa (Fig. 11C). The submucosa appears normal and does not display edema; the localization of neutrophils to this site suggests that the tissue is in the process of recovery. In POR2-infected mice, neutrophils localize once more to the lamina propria and the submucosa, in a pattern similar to that of RIMD2210633-infected mice but to a lesser extent (Fig. 11D). The ceca of POR3-infected mice appear normal and, accordingly, neutrophils are localized to the epithelium (Fig. 11E). The patterns of localization correlate strongly with tissue morphology in the infected samples; in a more inflamed tissue the neutrophils are prevalent in the disrupted mucosa and submucosa, while in healthier tissue localization is primarily at the epithelium.

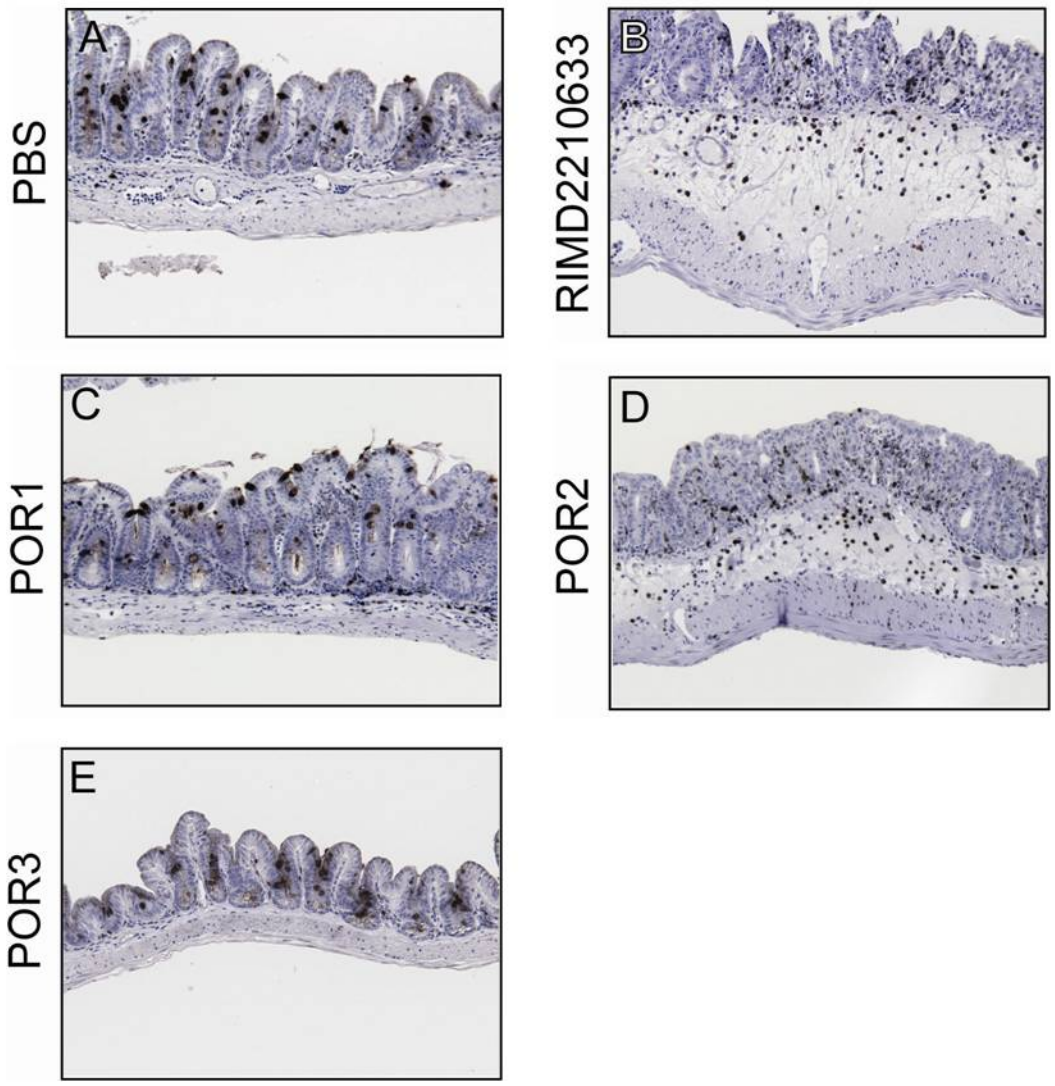

Figure 11. Neutrophils localize to sites of acute intestinal inflammation
Fixed, paraffin-embedded ceca from mice infected for 48 hours with (A) PBS, (B) RIMD2210633, (C) POR2, (D) POR2, or (E) POR3 were stained with an antibody against myeloperoxidase, a marker of neutrophils. All images are magnified 20X.

The crypt hyperplasia observed in hematoxylin and eosin-stained cecal tissue from *V. parahaemolyticus*-infected mice suggests that proliferation may occur as a step in the recovery and regeneration of ulcerated intestinal tissue. In order to characterize this process, we utilized immunofluorescence to detect staining of paraffin-embedded sections of cecal tissue with an antibody to Ki67, a marker of nuclear proliferation. In PBS-infected mice, proliferation is limited to a ring of cells lining the base of the single crypt layer (Fig. 12, A-C). When mice are infected with RIMD2210633, the cellular architecture of the cecum is obliterated by crypt ulceration at 24 hours, and proliferation is virtually absent (Fig. 12, D-F). In comparison, after 24 hours of infection with POR1 (Fig. 12, G-I) or POR2 (Fig. 12, J-L), the cellular architecture is more intact and consists predominantly of several crypt layers proliferating from the base of the mucosa. The architecture and Ki67 localization pattern in the ceca of POR3-infected mice (Fig. 12, M-O) appear normal and similar to the PBS control. Acute inflammation is present in POR1- and POR2-infected mice but recovery of the normal cellular architecture by crypt proliferation appears to occur earlier than in RIMD2210633-infected mice, an observation that is in accordance with results in Figures 9 and 12.

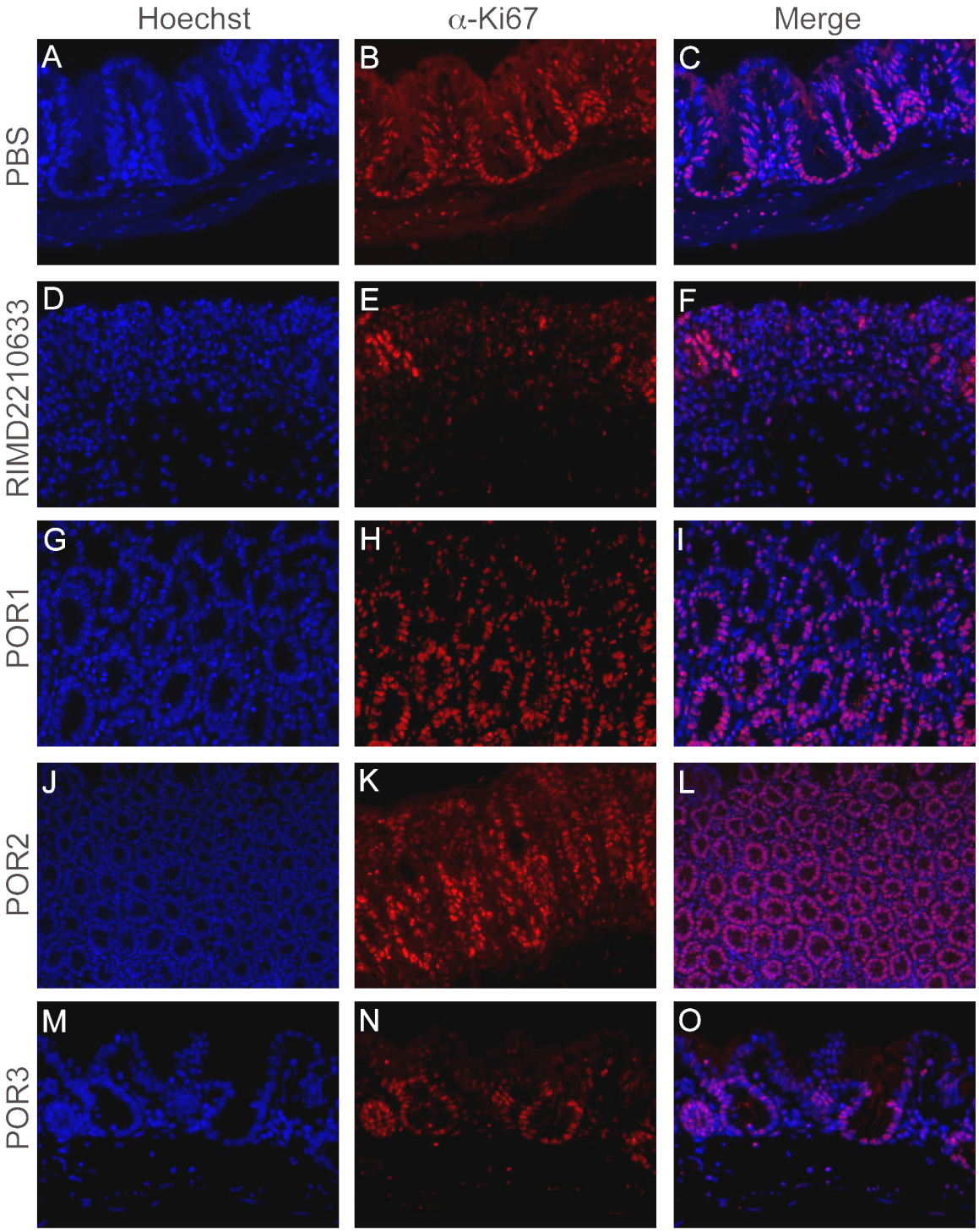
Hoechst
α-Ki67
Merge
PBS
RIMD2210633
POR1
POR2
POR3
A
B
C
D
E
F
G
H
I
J
K
L
M
N
O

Figure 12. Crypt proliferation in *V. parahaemolytius*-infected germfree mice (previous page).
Fixed, paraffin-embedded ceca from mice infected for 24 hours with (A-C) PBS, (D-F) RIMD2210633, (G-I) POR2, (J-L) POR2, or (M-O) POR3 were stained with an antibody against Ki67, a marker of nuclear proliferation, and counterstained with Hoechst. Antibody signal was amplified with a biotinylated secondary antibody and streptavidin-conjugated fluorophore. All images are magnified 20X.

Upregulation of inflammatory genes in response to infection by *V. parahaemolyticus*

The histological analyses performed in the preceding section provide valuable information for identification of the inflammatory response in *V. parahaemolyticus*-infected mice. However, a more in-depth characterization of the murine inflammatory response requires molecular analysis to identify the cell types and signaling molecules involved in mediating this response. To this end, we performed quantitative reverse transcriptase polymerase chain reaction (qRT-PCR) to analyze changes in the transcriptional regulation of certain cytokines and chemokines known to participate in the intestinal inflammatory response. Changes in the expression of each gene were calculated relative to expression in PBS-infected control mice.

The expression of the cytokine interleukin-1 beta (IL-1β), a central mediator of the inflammatory response, is increased by an average of approximately 1 log in the ceca of mice infected with RIMD2210633, POR1, and POR2 at 24 (Fig. 13A) and 48 (Fig. 13B) hours. IL-1β is also slightly upregulated in the ceca of POR3-infected mice, but to a lesser extent. The other cytokine analyzed, interferon-γ (IFN-γ), is again upregulated in RIMD2210633-, POR1-, and POR2-infected mice, and to a lesser extent in POR3-infected mice, at 24 hours (Fig. 13E). Interestingly, the expression of IFN-γ in mice infected with POR1, POR2, and POR3 is decreased to control levels by 48 hours but remains elevated in RIMD2210633-infected mice (Fig. 13F).

We also analyzed the expression of three inflammatory chemokines, KC, macrophage inflammatory protein 2-alpha (MIP-2α), and CXCL-9. KC, also known as IL-8, is upregulated in mice infected with POR1, POR2, and POR3 at 24 hours (Fig. 14A). KC is upregulated only very slightly in mice infected with RIMD2210633 mice at 24 hours, although expression increases at 48 hours (Fig. 14B). MIP-2α is also upregulated by an average of approximately 1 log in mice infected with RIMD2210633, POR1, or POR2 for 24 hours (Fig. 14C). By 48 hours, expression of MIP-2α has decreased to control levels in POR1- and POR2-infected mice while remaining elevated in RIMD2210633-infected mice (Fig. 14D). Finally, we analyzed the expression of CXCL-9, a chemokine that is

induced by the cytokine IFN-γ [64]. Much like MIP-2α, CXCL-9 is upregulated in RIMD2210633-, POR1-, and POR2-infected mice, and to a lesser extent in POR3-infected mice, at 24 hours (Fig. 14E). At 48 hours, CXCL-9 remains elevated in mice infected with RIMD2210633 but is expressed at levels similar to control in mice infected with POR1, POR2, and POR3 (Fig. 14F). Taken together, these data support separate but complementary roles for TDH and the T3SS2 in contributing to *V. parahaemolyticus*-induced intestinal inflammation.

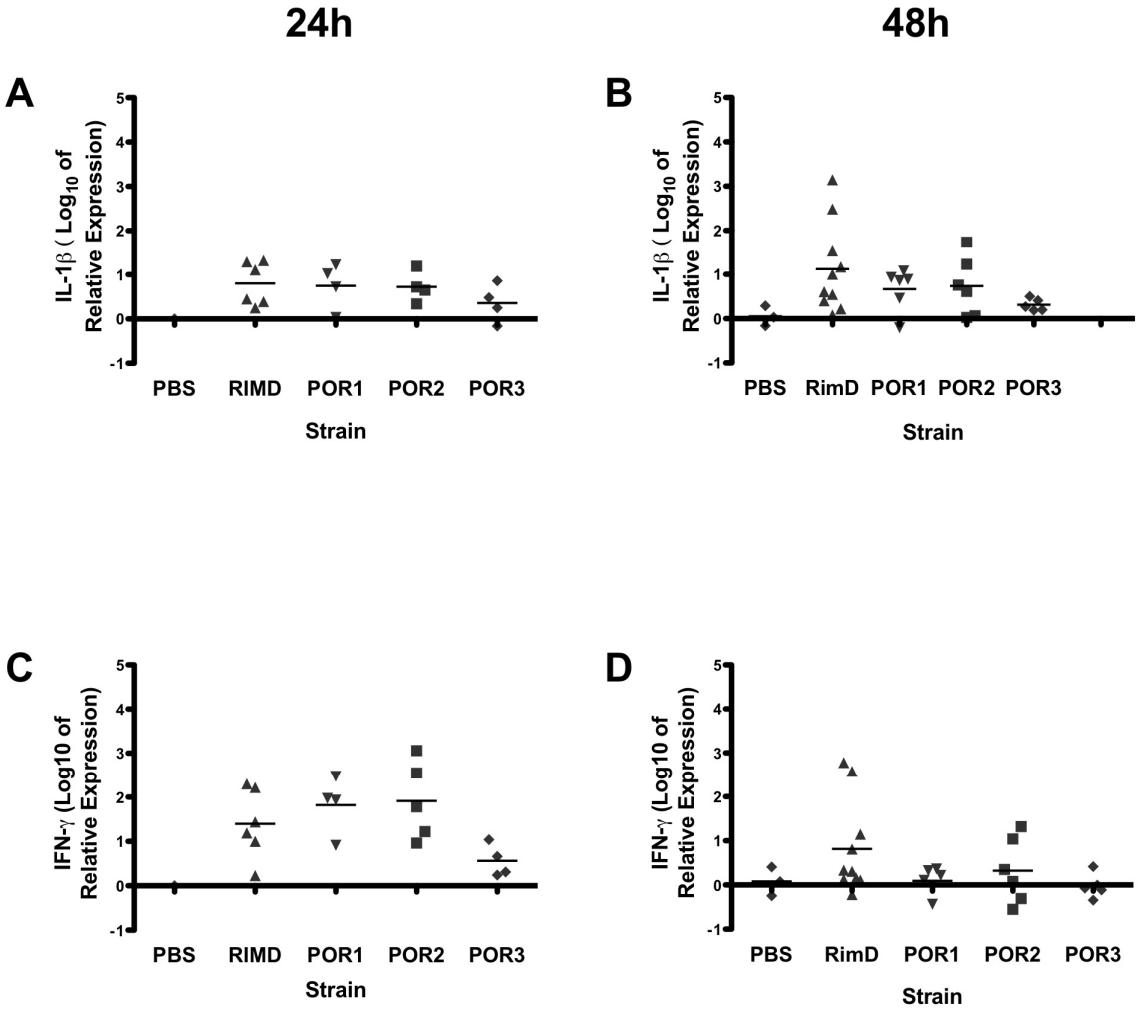

Figure 13. Expression of inflammatory cytokines in *V. parahaemolyticus*-infected mouse cecum

qRT-PCR analysis was performed on cecal tissue obtained from germfree mice infected for 24 or 48 hours with PBS or *V. parahaemolyticus*. Genes analyzed are as follows: (A-B) IL-1β, (C-D) IFN-γ.

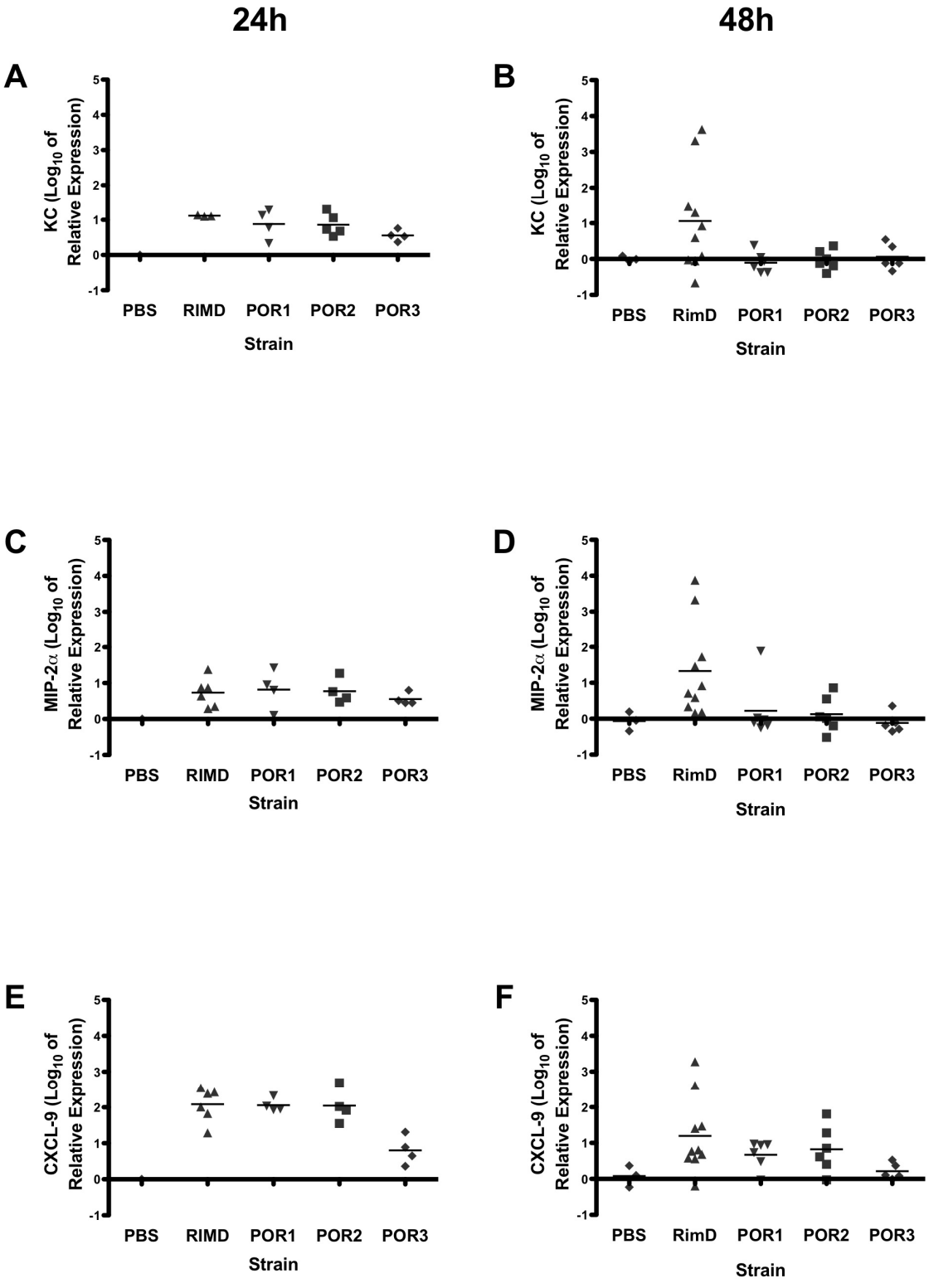
24h
48h
A
B
C
D
E
F
KC (Log10 of Relative Expression)
MIP-2α (Log10 of Relative Expression)
CXCL-9 (Log10 of Relative Expression)
PBS
RIMD
RimD
POR1
POR2
POR3
Strain

Figure 14. Expression of inflammatory chemokines in *V. parahaemolyticus*-infected mouse cecum (previous page)
qRT-PCR analysis was performed on cecal tissue obtained from germfree mice infected for 24 or 48 hours with PBS or *V. parahaemolyticus*. Genes analyzed are as follows: (A-B) KC, (C-D) MIP-2α, (E-F) CXCL-9.

Summary

In this study, we characterize the contributions of *V. parahaemolyticus* TDH and T3SS2 to enteropathogenesis *in vivo*. Infection of germfree mice with the wild type RIMD2210633 strain of *V. parahaemolyticus* results in inflammation characterized by submucosal edema, crypt ulceration and hyperplasia, and epithelial damage. During the first 24 hours of infection with POR1, which lacks TDH, a similar but attenuated response is observed. Infection with POR2, which lacks a functional T3SS1 but is otherwise identical to POR1, results in cecal inflammation that appears similar in magnitude to that of RIMD2210633 during the first 24 hours of infection but resolves more quickly than the wild type strain. Finally, infection with POR3, which lacks TDH and a functional T3SS2 but does possess a functional T3SS1, results in a phenotype intestinal phenotype that appears similar to a PBS-treated negative control. In addition to histological studies, qPCR analysis of the expression of inflammatory cytokines and chemokines demonstrate that these genes remain upregulated for a longer period of time in RIMD2210633-infected mice relative to mice infected with POR1 or POR2. Taken together, these data suggest that T3SS2 is required for

enterotoxicity and that TDH prolongs the inflammatory response during infection with *V. parahaemolyticus*.

CHAPTER FOUR
Conclusions

Discussion

V. parahaemolyticus-induced gastroenteritis is a growing problem worldwide, as evidenced by increasing numbers of outbreaks and the emergence of pandemic strains. While great progress has been made in characterizing virulence mechanisms such as TDH and type III secreted effectors *in vitro*, the lack of a suitable animal model has hampered our understanding of the full contribution of these mechanisms to the infection process. By establishing a system for the infection of adult germfree mice with *V. parahaemolyticus*, we have bypassed many of the limitations of systems currently used for the study of this pathogen *in vivo*.

Colonization resistance is often a complicating factor in the establishment of infection by pathogens in the murine gastrointestinal tract. In our studies, for example, the presence of indigenous microbiota precludes colonization of the intestine by *V. parahaemolyticus* in conventionally raised mice (Fig. 7). By using germfree mice, we are able to bypass the microbial competition that *V. parahaemolyticus* would otherwise face. An alternative approach, popularized before the advent of accessible germfree technology, involves pretreatment of the animal with antibiotics to clear the intestinal environment [66]. However, this

approach cannot guarantee that the intestine will be completely sterile. The introduction of *V. parahaemolyticus* to an otherwise sterile intestinal environment allows for more confidence in attributing any inflammatory effects observed to this pathogen.

Colonization of the germfree mouse intestine by the mutant POR strains of *V. parahaemolyticus*, in addition to the clinical isolate RIMD2210633, suggests that colonization is not dependent on TDH or the T3SSs. Indeed, germfree mice are successfully colonized by a wide range of different bacteria, pathogenic or not [29]. While some translocation of RIMD2210633 to the mesenteric lymph was detected, *V. parahaemolyticus* was largely absent from the MLN and spleen, suggesting that infection by *V. parahaemolyticus* is acute and localized to the intestine.

Infection of germfree mice with the wild-type *V. parahaemolyticus* clinical isolate RIMD2210633 results in cecal inflammation characterized by submucosal edema, crypt ulceration and hyperplasia, epithelial damage, and infiltration by neutrophils into the submucosa and lamina propria. Similar signs of inflammation are also present in the ceca of mice infected with POR1 and POR2, but not POR3. From these phenotypes it may be inferred that a functional T3SS2, which is present in POR1 and POR2 but not in POR3, contributes to *V. parahaemolyticus*-induced enteropathogenesis. Of the three virulence factors—TDH, T3SS1, and T3SS2—that are present in wild-type RIMD2210633, only

T3SS1 is functional in the mutant strain POR3. The lack of an inflammatory phenotype in the ceca of mice infected with POR3 suggests that T3SS1 does not contribute to the enteropathogenesis of *V. parahaemolyticus*. However, it is interesting to note that, 24 hours post infection, the inflammatory response elicited by POR2, in which only T3SS2 is functional, actually appears more severe than that elicited by POR1, which contains both functional T3SSs (Fig. 9, compare panels G and E). These data imply that T3SS1 may attenuate the inflammatory phenotype elicited by T3SS2. While additional work will be required to determine the mechanism or mechanisms by which this attenuation occurs, existing studies on T3SS1 and T3SS2 may provide some direction in answering this question. As discussed previously, T3SS1, but not T3SS2, was shown to induce cytotoxicity in a cell culture model [9, 34], while T3SS2, but not T3SS1, was shown to be responsible for the enterotoxicity observed in the rabbit ileal loop model. When T3SS1 and T3SS2 are both present and functional, as is the case in POR1, T3SS1-mediated cytotoxicity may counteract T3SS2-mediated cellular proliferation so that general inflammation is tempered. Indeed, the level of crypt proliferation in POR2, as measured by immunostaining for Ki67, exceeds that of POR1 (Fig. 13, compare panels J-L to panels G-I).

Of the many unanswered questions surrounding virulence mechanisms of *V. parahaemolyticus*, one of the most prominent regards the role of TDH. While activity of TDH *in vitro* has been characterized by several groups [42], its

requirement for enterotoxicity *in vivo* is controversial. Park *et al* demonstrated that the POR1 mutant strain of *V. parahaemolyticus*, which lacks TDH and TRH, was enterotoxic in the rabbit ileal loop system [46], even though at least one of these hemolysins was long thought to be required for enterotoxicity (REFs). In these studies, we demonstrate separate but complementary roles for TDH and T3SS2 in the induction of acute inflammation in the germfree mouse intestine.

Germfree mice infected with RIMD2210633 for 24 or 48 hours exhibit severe cecal inflammation (Fig. 9, panels C-D; Fig.10). While similar inflammation may also be seen in the ceca of mice infected with POR2 for 24 hours (Fig. 9G), by 48 hours much of this inflammation has already been resolved (Fig. 9H). The pattern of Ki67 staining at 48 hours also reflects this trend (Fig. 13, panels D-F), suggesting that crypt proliferation and resolution of inflammation are delayed in RIMD2210633 relative to POR2. POR2 lacks both TDH and a functional T3SS1; however, the POR1 phenotype discussed previously suggests that T3SS1, rather than prolonging inflammation, would actually have the opposite effect during infection by attenuating enterotoxicity. It may thus be concluded that TDH acts in some fashion to prolong *V. parahaemolyticus*-mediated inflammation. If so, a number of possibilities exist to explain the kinetics of the TDH contribution. For example, T3SS2 may elicit inflammation during the early stages of infection while TDH acts later; alternatively, both T3SS2 and TDH may act concurrently at the start of infection but TDH is either

active for a longer period of time or elicits such a strong inflammatory response that resolution is delayed. Analysis of the timing of infection-mediated inflammatory gene expression may address this question.

At 24 hours, the expression of the cytokines IL-1β and IFN-γ, and of the chemokines KC, MIP-2α and CXCL-9, are increased by one to two logs in POR1- and POR2-infected mice (Figs. 14-15). All of these genes, with the exception of KC, are also upregulated in RIMD2210633-infected mice at 24 hours. By 48 hours, the expression of every gene analyzed has decreased in the POR1- and POR2-infected mice. However, expression of these genes in RIMD2210633-infected mice remains elevated or even increases at 48 hours, supporting the idea that TDH prolongs inflammation in some fashion. More telling, perhaps, is the delayed upregulation of KC in RIMD2210633-infected cecum, which suggests that during infection the inflammatory action of TDH takes effect later than that of T3SS2. KC functions as a chemokine to recruit neutrophils and other leukocytes to the site of inflammation [4], so delayed upregulation suggests that this recruitment and the eventual resolution of inflammation are also delayed in the presence of TDH.

Analysis of changes in inflammatory gene expression and the functions of these genes may also illuminate the inflammatory process in the intestinal tissue of infected mice. The cytokines IL-1β and IFN-γ, for example, exert a variety of biological effects as regulators of gene expression, upregulating additional

cytokines and inflammatory mediators while downregulating housekeeping genes in response to immunological challenge [14, 61]. Both IL-1β and IFN-γ have been shown to disrupt intestinal epithelial tight junctions, which represent a crucial component of the intestinal barrier defense system [2]. Disruption of tight junctions facilitates the translocation of bacteria and bacterial antigens across the epithelial barrier and into the underlying intestinal tissue, where the immunological response is amplified by the production of additional cytokines and chemokines [13, 37, 63]. The upregulation of chemokines and subsequent recruitment of leukocytes, such as neutrophils, may in turn stimulate the eventual resolution of inflammation through the clearance of necrotic tissue and cellular debris.

The sterility of the gastrointestinal tract of the germfree mouse is advantageous for reasons previously discussed but also presents a potential drawback in that any immune reaction elicited may be a general response to the introduction of foreign microbes rather than a specific response to *V. parahaemolyticus*. However, infection with the POR3 strain of *V. parahaemolyticus*, which lacks the virulence factors thought to contribute to enteropathogenesis, does not appear to elicit a notable inflammatory response. Infection with POR3 may therefore be considered a *V. parahaemolyticus* negative control for enteropathogenicity in this model and indirectly affirms the results obtained with the other, enteropathogenic strains of *V. parahaemolyticus*.

In summary, we have established an *in vivo* model of infection by the pathogen *V. parahaemolyticus* in germfree mice. The intestinal inflammation induced by infection with *V. parahaemolyticus* is characterized by submucosal edema, crypt ulceration and hyperplasia, epithelial damage, and infiltration by neutrophils into the submucosa and lamina propria; these phenotypes are also characteristic of intestinal tissue samples isolated from humans infected with *V. parahaemolyticus*. Our studies demonstrate that TDH and T3SS2 play separate but complementary roles in induction of the inflammatory response, with T3SS2 required for enterotoxicity and TDH prolonging inflammation. Consistent with previous studies, T3SS1 is not required for the enterotoxic effects of *V. parahaemolyticus* and may actually, through its ability to induce cytotoxicity, attenuate the enterotoxicity of T3SS2.

Future Directions

The establishment of a system for the infection of germfree mice with *V. parahaemolyticus* presents a useful tool for the further study of this pathogen. A number of experiments may be proposed to evaluate the robustness of this system. For example, we have demonstrated in these studies that, in the absence of TDH, resolution of intestinal inflammation begins to occur between 24 to 48 hours of infection with *V. parahaemolyticus*. As oral infection with this pathogen in humans is generally self-limiting and not lethal, longer time courses of infection

will be required to determine the full duration of intestinal inflammation as well as clearance of the pathogen by the intestinal tract and immune system. Additionally, more accurate simulation of the human intestinal environment may be achieved by colonizing germfree mice with components of human microflora prior to infection with *V. parahaemolyticus*. While the intestinal microbes indigenous to conventionally raised mice effectively outcompete *V. parahaemolyticus* and infection of germfree mice might be deemed artificial, colonization with human microflora may represent a happy medium between these two extremes.

The results obtained in this study also raise a number of questions regarding the virulence mechanisms of *V. parahaemolyticus*. The mechanism by which TDH contributes to enteropathogenicity, while partially elucidated here, remains ever mysterious. Experiments in which TDH can be studied in isolation will be required to address this question; possible approaches include oral delivery of purified TDH to the mouse or infection with a TDH-positive strain lacking functional T3SSs. As purified TDH is lethal even to conventionally raised mice [30], administration to germfree mice is not likely to be informative. The latter option represents a more feasible approach, although such a strain of *V. parahaemolyticus* does not occur in nature and would have to be engineered. This approach may also be useful in elucidating the effects of individual effectors of *V. parahaemolyticus* through the use of knockout strains. A potential complement to

this approach involves the use of a heterologous system in which individual *V. parahaemolyticus* effectors are secreted from an effectorless strain of *Yersinia* spp. While the introduction of a another bacterium may confound the effects of the effector or effectors in question, this approach may also be more informative than the subtractive method employed by the use of knockouts. Finally, the study of the mechanistic contributions of individual effectors may also come full circle by elucidating the relative contributions of T3SS1 and T3SS2.

BIBLIOGRAPHY

1. **Imaoka, A., Matsumoto, S., Setoyama, H., Okada, Y., and Y. Umesaki.** 1996. Proliferative recruitment of intestinal intraepithelial lymphocytes after microbial colonization of germ-free mice. Eur J Immunol **26**:945-948.

2. **Al-Sadi, R., Boivin, M., and T. Ma.** 2009. Mechanism of cytokine modulation of epithelial tight junction barrier. Front Biosci. **14**:2765-78.

3. **Asano, T.** 1969. Anion concentration in cecal content of germfree and conventional mice. Proc Soc Exp Biol Med **131**:1201-5.

4. **Baggiolini, M. and I. Clark-Lewis.** 1992. Interleukin-8, a chemotactic and inflammatory cytokine. FEBS Lett **307**:97-101.

5. **Black, D. and J.B. Bliska.** 2000. The RhoGAP activity of the *Yersinia pseudotuberculosis* cytotoxin YopE is required for antiphagocytic function and virulence. Mol Microbiol **37**:515-527.

6. **Boyd, J.F.** 1985. Pathology of the alimentary tract in *Salmonella typhimurium* food poisoning. Gut **26**:935-944.

7. **Brown, D.F., Spaulding, P.L., and R.M. Twedt.** 1977. Enteropathogenicity of *Vibrio parahaemolyticus* in the ligated rabbit ileum. Appl Environ Microbiol **33**:10-14.

8. **Bruckner-Kardoss, E. and B.S. Wostmann.** 1967. Cecectomy of germfree rats. Lab Anim Care **17**:542-546.

9. **Burdette, D.L., Yarbrough, M.L., Orvedahl, A., Gilpin, C.J., and K. Orth.** 2008. *Vibrio parahaemolyticus* orchestrates a multifaceted host cell infection by induction of autophagy, cell rounding, and then cell lysis. Proc Natl Acad Sci USA **105**:12497-12502.

10. **Daniels, N.A., Mackinnon, L., Bishop, R., Altekruse, S., Ray, B., Hammond, R.M., Thompson, S., Wilson, S., Bean, N.H., Griffin, P.M., and L. Slutsker.** 2000. *Vibrio parahaemolyticus* Infections in the United States, 1973-1998. J Infect Dis **181**:1661-1666.

11. **De, S.N.** 1959. Enterotoxicity of Bacteria-free Culture-filtrate of *Vibrio cholerae.* Nature **183**:1533-1534.

12. **De, S.N. and D.N. Chatterje.** 1953. An experimental study of the mechanism of action of *vibrio choleræ* on the intestinal mucous membrane. J Pathol Bacteriol **66**:559-562.

13. **DeMeo, M.T., Mutlu, E.C., Keshavarzian, A., and M.C. Tobin.** 2002. Intestinal permeation and gastrointestinal disease. J Clin Gastroenterol **34**:385-96.

14. **Dinarello, C.** 1994. The interleukin-1 family: 10 years of discovery. FASEB J **8**:1314-1325.

15. **Panina, E.M., S.M., Griffith, N., Kozak, N.A., Yuk, M.H., Miller, J.F.** 2005. A genome-wide screen identifies a Bordetell type III secretion effector and candidate effectors in other species. Mol Microbiol **58**:267-279.

16. **Engel, J. and P. Balachandran.** 2009. Role of *Pseudomonas aeruginosa* type III effectors in disease. Curr Opin Microbiol **12**:61-66.

17. **Fabbri, A., Falzano, L., Frank, C., Donelli, G., Matarrese, P., Raimondi, F., Fasano, A., and C. Fiorentini.** 1999. *Vibrio parahaemolyticus* Thermostable Direct Hemolysin Modulates Cytoskeletal Organization and Calcium Homeostasis in Intestinal Cultured Cells. Infect Immun **67**:1139-1148.

18. **Fujino, T., Okuno, Y., Nakada, D., Aoyama, A., K. Fukai, K., Mukai, T., and T. Ueho.** 1953. On the bacteriological examination of Shirasu-food poisoning. Med J Osaka Univ **4**:299-304.

19. **Galan, J.E. and H. Wolf-Watz.** 2006. Protein delivery into eukaryotic cells by type III secretion machines. Nature **444**:567-573.

20. **Gordon, H.A., Bruckner-Kardoss, E., and B.S. Wostmann.** 1966. Aging in Germ-free Mice: Life Tables and Lesions Observed at Natural Death. J Gerontol **21**:380-387.

21. **Gordon, H.A. and L. Pesti.** 1971. The gnotobiotic animal as a tool in the study of host microbial relationships. Microbiol Mol Biol Rev **35**:390-429.

22. **Gordon, H.A. and B.S. Wostmann.** 1973. Chronic mild diarrhea in germfree rodent: a model portraying host-flora synergism, in *Germfree Research: Biological Effects of Gnotobiotic Environments*, J. Heneghan, Editor. New York: Academic, pp. 593-601.

23. **Tang, G.Q., Iida, T., Yamamoto, K., and T. Honda.** 1995. Ca^{2+}-independent cytotoxicity of *Vibrio parahaemolyticus* thermostable direct hemolysin (TDH) on Intestine 407, a cell line derived from human embryonic intestine. FEMS Microbiol Lett **134**:233-238.

24. **Hertzog, M., van Heijenoort, C., Didry,D., Gaudier M., Coutant,J., Gigant, B.T., Didelot, G., Préat, T., Knossow, M., Guittet, E., and M.-F. Carlier.** 2004. The β-Thymosin/WH2 Domain: Structural Basis for the Switch from Inhibition to Promotion of Actin Assembly. Cell **117**:611-623.

25. **Hoashi K, O.K., Taniguchi H, Yamashita H, Tsuji K, Mizuguchi Y, Ohtomo N.** 1990. Pathogenesis of *Vibrio parahaemolyticus:* intraperitoneal and orogastric challenge experiments in mice. Microbiol Immunol **34**:355-366.

26. **Honda, S., Goto, I., Minematsu, I., Ikeda, N., Asano, N., Ishibashi, M., Kinoshita, Y., Nishibuchi, M., Honda, T., Miwatani, T.** 1987. Gastroenteritis due to Kanagawa negative *Vibrio parahaemolyticus.* Lancet **329**:331-332.

27. **Honda, T., Y.X. Ni, and T. Miwatani.** 1988. Purification and characterization of a hemolysin produced by a clinical isolate of Kanagawa phenomenon-negative *Vibrio parahaemolyticus* and related to the thermostable direct hemolysin. Infect Immun **56**:961-965.

28. **Honda, T., Ni, Y., Miwatani, T., Adachi, T., Kim, J.** 1992. The thermostable direct hemolysin of *Vibrio parahaemolyticus* is a pore forming toxin. Can J Microbiol **38**:1175-1180.

29. **Hooper, L.V., M.H. Wong, A. Thelin, L. Hansson, P.G. Falk, and J.I. Gordon.** 2001. Molecular Analysis of Commensal Host-Microbial Relationships in the Intestine. Science **291**:881-884.

30. **Iida, T., Honda, T.** 1997. Hemolysins produced by vibrios. J Toxicol Toxin Rev **16**:216-227.

31. **Kaneko, T. and R.R. Colwell.** 1973. Ecology of *Vibrio parahaemolyticus* in Chesapeake Bay. J. Bacteriol. **113**:24-32.

32. **Krantz, G.E., Colwell, R.R., and E. Lovelace.** 1969. *Vibrio parahaemolyticus* from the Blue Crab *Cailinectes sapidus* in Chesapeake Bay. Science **164**:1286-1287.

33. **Kubori, T., Matsushima, Y., Nakamura, D., Uralil, J., Lara-Tejero, M., Sukhan, A., Galan, J.E., and S.-I. Aizawa.** 1998. Supramolecular Structure of the *Salmonella typhimurium* Type III Protein Secretion System. Science **280**:602-605.

34. **Liverman, A.D.B., Cheng, H.-C., Trosky, J.E., Leung, D.W., Yarbrough, M.L., Burdette, D.L., Rosen, M.K., and K. Orth.** 2007. Arp2/3-independent assembly of actin by *Vibrio* type III effector VopL. Proc Nat Acad Sci USA **104**:17117-17122.

35. **Nishibuchi, M. and J.B. Kaper.** 1990. Duplication and variation of the thermostable direct haemolysin (tdh) gene in *Vibrio parahaemolyticus.* Mol Microbiol **4**:87-99.

36. **Makino, K., Oshima, K., Kurokawa, K., Yokoyama, K., Uda, T., Tagomori, K., Iijima, Y., Najima, M., Nakano, M., Yamashita, A., Kubota, Y., Kimura, S., Yasunaga, T., Honda, T., Shinagawa, H., Hattori, M., and T. Iida.** 2003. Genome sequence of *Vibrio parahaemolyticus:* a pathogenic mechanism distinct from that of *V. cholerae.* Lancet **361**:743-749.

37. **Bruewer, M., Samarin, S., and A. Nusrat.** 2006. Inflammatory Bowel Disease and the Apical Junctional Complex. Ann NY Acad Sci **1072**:242-252.

38. **McLaughlin, J.B., Depaola, A., Bopp, C.A., Martinek, K.A., Napolilli, N.P., Allison, C.G., Murray, S.L., Thompson, E.C., Bird, M.M., and J.P. Middaugh.** 2005. Outbreak of *Vibrio parahaemolyticus* Gastroenteritis Associated with Alaskan Oysters. N Engl J Med **353**:1463-1470.

39. **Miyamoto, Y., Kato, T., Obara, Y., Akiyama, S., Takizawa, K., and S. Yamai.** 1969. In Vitro Hemolytic Characteristic of *Vibrio parahaemolyticus:* Its Close Correlation with Human Pathogenicity. J Bacteriol **100**:1147-1149.

40. **Molenda, J.R., Johnson, W.G., Fishbein, M., Wentz, B., Mehlman, I.J., and T.A. Dadisman.** 1972. *Vibrio parahaemolyticus* Gastroenteritis in Maryland: Laboratory Aspects. Appl Microbiol **24**:444-448.

41. **Mukherjee, S., Keitany, G., Li, Y., Wang, Y., Ball, H.L., Goldsmith, E.J., and K. Orth.** 2006. *Yersinia* YopJ Acetylates and Inhibits Kinase Activation by Blocking Phosphorylation. Science **312**:1211-1214.

42. **Nishibuchi, M. and J.B. Kaper.** 1995. Thermostable direct hemolysin gene of *Vibrio parahaemolyticus*: a virulence gene acquired by a marine bacterium. Infect Immun **63**:2093-2099.

43. **Okuda, J., Ishibashi, M., Hayakawa, E., Nishino, T., Takeda, Y., Mukhopadhyay, A.K., Garg, S., Bhattacharya, S.K., Nair, G.B., and M. Nishibuchi.** 1997. Emergence of a unique O3:K6 clone of *Vibrio parahaemolyticus* in Calcutta, India, and isolation of strains from the same clonal group from Southeast Asian travelers arriving in Japan. J Clin Microbiol **35**:3150-3155.

44. **Ono, T., Park, K.-S., Ueta, M., Iida, T., and T. Honda.** 2006. Identification of Proteins Secreted via *Vibrio parahaemolyticus* Type III Secretion System 1. Infect Immun **74**:1032-1042.

45. **Park, K.-S., Ono, T., Rokuda, M., Jang, M.-H., Iida, T., and T. Honda.** 2004. Cytotoxicity and Enterotoxicity of the Thermostable Direct Hemolysin-Deletion Mutants of *Vibrio parahaemolyticus*. Microbiol Immunol **48**:313-318.

46. **Park, K.-S., Ono, T., Rokuda, M., Jang, Okada, K., Iida, T., and T. Honda.** 2004. Functional Characterization of Two Type III Secretion Systems of *Vibrio parahaemolyticus*. Infect Immun **72**:6659-6665.

47. **Pasteur, L.** 1885. Observations relatives a la Note precedente de M. Declaux. C R Acad Sci Paris **100**:68.

48. **Qadri, F., Alam, M.S., Nishibuchi, M., Rahman, T., Alam, N.H., Chisti, J., Kondo, S., Sugiyama, J., Bhuiyan, N.A., Mathan, M.A., Sack, D.A., and G.B. Nair.** 2003. Adaptive and Inflammatory Immune Responses in Patients Infected with Strains of *Vibrio parahaemolyticus*. J Infect Dis **187**:1085-1096.

49. **Quinlan, M.E., Heuser, J.E., Kerkhoff, E., and R.D. Mullins.** 2005. *Drosophila* Spire is an actin nucleation factor. Nature **433**:382-388.

50. **Raimondi, F., Kao, J.P.Y., Fiorentini, C., Fabbri, A., Donelli, G., Gasparini, N., Rubino, A., and A. Fasano.** 2000. Enterotoxicity and Cytotoxicity of *Vibrio parahaemolyticus* Thermostable Direct Hemolysin in In Vitro Systems. Infect Immun **68**:3180-3185.

51. **Reyniers, J.A., Trexler, P.C., Ervin, R.F., Wagner, M., Luckey, T.D., and H.A. Gordon.** 1949. A complete life-cycle in the germfree Bantam chicken. Nature **163**:67-68.

52. **Reyniers, J.A., Trexler, P.C., Ervin, R.F., Wagner, M., Luckey, T.D., and H.A. Gordon.** *The need for a unified terminology in germfree life studies*, in *Lobund reports no. 2*, J.A. Reyniers, Editor. 1949, University of Notre Dame Press: Notre Dame, IN. p. 151-162.

53. **Reyniers, J.A., Trexler, P.C., and R.F. Ervin.** *Rearing germfree albino rats*, in *Lobund reports no. 1*, J.A. Reyniers, Editor. 1946, University of Notre Dame Press: Notre Dame, IN. p. 2-84.

54. **Rosqvist, R., Forsberg, Å., Rimpiläinen, M., Bergman, T., and H. Wolf-Watz.** 1990. The cytotoxic protein YopE of *Yersinia* obstructs the primary host defence. Mol Microbiol **4**:657-667.

55. **Rosqvist, R., A. Forsberg, and H. Wolf-Watz.** 1991. Intracellular targeting of the *Yersinia* YopE cytotoxin in mammalian cells induces actin microfilament disruption. Infect Immun **59**:4562-4569.

56. **Rosqvist, R., Magnusson, K.E., and H. Wolf-Watz.** 1994. Target cell contact triggers expression and polarized transfer of *Yersinia* YopE cytotoxin into mammalian cells. EMBO J **13**:964-972.

57. **Sakazaki, R., Tamura, K., Nakamura, A., Kurata, T., Ghoda, A., and Kazuno.** 1974. Studies on enteropathogenic activity of *Vibrio parahaemolyticus* using ligated gut loop model in rabbits. Jpn J Med Sci Biol **27**:35-43.

58. **Sakurai, J., Honda, T., Jinguji, Y., Arita, M., and T. Miwatani.** 1976. Cytotoxic effect of the thermostable direct hemolysin produced by Vibrio parahaemolyticus on FL cells. Infect. Immun. **13**:876-883.

59. **Santos, R.L., Zhang, S., Tsolis, R.M., Kingsley, R.A., Adams, L.G., and A.J. Bäumler.** Animal models of *Salmonella* infections: enteritis versus typhoid fever. Microb Infect **3**:1335-1344.

60. **Schmidt, G., Sehr, P., Wilm, M., Selzer, J., Mann, M., and K. Aktories.** 1997. Gln63 of Rho is deamidated by *Escherichia coli* cytotoxic necrotizing factor-1. Nature **387**:725-729.

61. **Schroder, K., Hertzog, P.J., Ravasi, T., and D.A. Hume.** 2004. Interferon-γ: an overview of signals, mechanisms and functions. J Leukoc Biol **75**:163-189.

62. **Shehan, D.C. and B.B. Hrapchak.** *Theory and Practice of Histotechnology*. 2nd ed. 1980: Battelle Press.

63. **Shen, L. and J.R. Turner.** 2006. Role of Epithelial Cells in Initiation and Propagation of Intestinal Inflammation. Eliminating the static: tight junction dynamics exposed. Am J Physiol Gastrointest Liver Physiol **290**:G577-582.

64. **Singh, U.P., Venkataraman, C., Singh, R., and J.W. Lilliard, Jr.** 2007. CXCR3 Axis: Role in Inflammatory Bowel Disease and its Therapeutic Implication. Endocr Metab Immune Disord: Drug Targets **7**:111-123.

65. **Skelly, B.J., Trexler, P.C., and J. Tanami.** 1962. Effect of a *Clostridium* species upon cecal size of gnotobiotic mice. Proc Soc Exp Biol Med **110**:455-458.

66. **Stecher, B., Macpherson, A.J., Hapfelmeier, S., Kremer, M., Stallmach, T., and W.-D. Hardt.** 2005. Comparison of *Salmonella enterica* Serovar *Typhimurium* Colitis in Germfree Mice and Mice Pretreated with Streptomycin. Infect Immun **73**:3228-3241.

67. **Takahashi, A., Kenjyo, N., Imura, K., Myonsun, Y., and T. Honda.** 2000. Cl- Secretion in Colonic Epithelial Cells Induced by the *Vibrio parahaemolyticus* Hemolytic Toxin Related to Thermostable Direct Hemolysin. Infect Immun **68**:5435-5438.

68. **Takahashi, A., Sato, Y., Shiomi, Y., Cantarelli, V.V., Iida, T., Lee, M., and T. Honda.** 2000. Mechanisms of chloride secretion induced by thermostable direct haemolysin of *Vibrio parahaemolyticus* in human

colonic tissue and a human intestinal epithelial cell line. J Med Microbiol **49**:801-810.

69. **Takeda, Y., Taga, S., and T. Miwatani.** 1978. Evidence that thermostable direct hemolysin of *Vibrio parahaemolyticus* is composed of two subunits. FEMS Microbiol Lett **4**:271-274.

70. **Kodama, T., Rokuda, M., Park, K.-S., Cantarelli, V.V., Matsuda, S., Iida, T., and T. Honda,.** 2007. Identification and characterization of VopT, a novel ADP-ribosyltransferase effector protein secreted via the *Vibrio parahaemolyticus* type III secretion system 2. Cell Microbiol **9**:2598-2609.

71. **Trosky, J.E., Li, Y., Mukherjee, S., Keitany, G., Ball, H., and K. Orth.** 2007. VopA Inhibits ATP Binding by Acetylating the Catalytic Loop of MAPK Kinases. J Biol Chem **282**:34299-34305.

72. **Twedt, R.M., and D.F. Brown.** Studies on the enteropathogenicity of Vibrio parahaemolyticus in the ligated rabbit ileum, in *International symposium on Vibrio parahaemolyticus*. 1974. Tokyo: Saikon Publishing Co.

73. **Twedt, R.M., Peeler, J.T., and P.L. Spaulding.** 1980. Effective ileal loop dose of Kanagawa-positive *Vibrio parahaemolyticus*. Appl Environ Microbiol **40**:1012-1016.

74. **Ujiye, K.K.** 1970. Protective effect on infections with *Vibrio cholerae* in suckling mice caused by the passive immunization with milk of immune mothers. J Infect Dis **121**:50+.

75. **von Pawel-Rammingen, U., Telepnev M.V., Schmidt, G., Aktories, K., Wolf-Watz, H., and R. Rosqvist,.** 2000. GAP activity of the *Yersinia* YopE cytotoxin specifically targets the Rho pathway: a mechanism for disruption of actin microfilament structure. Mol Microbiol **36**:737-748.

76. **Umesaki, Y., Setoyama, H., Matsumoto, S., and Y. Okada.** 1993. Expansion of αβ T-cell receptor-bearing intestinal intraepithelial lymphocytes after microbial colonization in germ-free mice and its independence from thymus. Immunology **79**:32-37.

77. **Vongxay, K., Wang, S., Zhang, X., Wu, B., Hu, H., Pan, Z., Chen, S., and W. Fang.** 2008. Pathogenetic characterization of *Vibrio*

parahaemolyticus isolates from clinical and seafood sources. Int J Food Microbiol **126**:71-75.

78. **Waaij, D.V.D.** 1989. The Ecology of the Human Intestine and its Consequences for Overgrowth by Pathogens such as *Clostridium Difficile.* Ann Rev Microbiol **43**:69-87.

79. **Woods, A.E. and R.C. Ellis.** *Laboratory Histopathology, A Complete Reference* 1996: Churchill - Livingston Press.

80. **Wostmann, B.S., Reddy, B.S., Bruckner-Kardoss, E., Gordon, H.A., and B. Singh.** Causes and possible consequences of cecal enlargement in germfree rats, in *Germfree Research: Biological Effects of Gnotobiotic Environments*, J. Heneghan, Editor. 1973, Academic: New York. p. 261-70.

81. **Yarbrough, M.L., Li, Y., Kinch, L.N., Grishin, N.V., Ball, H.L., and K. Orth.** 2009. AMPylation of Rho GTPases by *Vibrio* VopS Disrupts Effector Binding and Downstream Signaling. Science **323**:269-272.

82. **Yeung, P.S.M. and K.J. Boor.** 2004. Epidemiology, Pathogenesis, and Prevention of Foodborne *Vibrio parahaemolyticus* Infections. Foodborne Pathog Dis **1**:74-88.